LETTER

doi:10.1038/nature10348

Ebola virus entry requires the cholesterol transporter Niemann–Pick C1

Jan E. Carette[1]†*, Matthijs Raaben[2]*, Anthony C. Wong[3]*, Andrew S. Herbert[4], Gregor Obernosterer[1]†, Nirupama Mulherkar[3], Ana I. Kuehne[4], Philip J. Kranzusch[2], April M. Griffin[2], Gordon Ruthel[4], Paola Dal Cin[5], John M. Dye[4], Sean P. Whelan[2], Kartik Chandran[3] & Thijn R. Brummelkamp[1]†

Infections by the Ebola and Marburg filoviruses cause a rapidly fatal haemorrhagic fever in humans for which no approved antivirals are available[1]. Filovirus entry is mediated by the viral spike glycoprotein (GP), which attaches viral particles to the cell surface, delivers them to endosomes and catalyses fusion between viral and endosomal membranes[2]. Additional host factors in the endosomal compartment are probably required for viral membrane fusion; however, despite considerable efforts, these critical host factors have defied molecular identification[3–5]. Here we describe a genome-wide haploid genetic screen in human cells to identify host factors required for Ebola virus entry. Our screen uncovered 67 mutations disrupting all six members of the homotypic fusion and vacuole protein-sorting (HOPS) multisubunit tethering complex, which is involved in the fusion of endosomes to lysosomes[6], and 39 independent mutations that disrupt the endo/lysosomal cholesterol transporter protein Niemann–Pick C1 (NPC1)[7]. Cells defective for the HOPS complex or NPC1 function, including primary fibroblasts derived from human Niemann–Pick type C1 disease patients, are resistant to infection by Ebola virus and Marburg virus, but remain fully susceptible to a suite of unrelated viruses. We show that membrane fusion mediated by filovirus glycoproteins and viral escape from the vesicular compartment require the NPC1 protein, independent of its known function in cholesterol transport. Our findings uncover unique features of the entry pathway used by filoviruses and indicate potential antiviral strategies to combat these deadly agents.

We have developed haploid genetic screens to gain insight into the biological processes relevant to human disease[8,9]. Here we use this approach to explore the filovirus entry pathway at an unprecedented level of detail. To interrogate millions of gene disruption events for defects in Ebola virus entry, we used a replication-competent vesicular stomatitis virus bearing the Ebola virus glycoprotein (rVSV-GP-EboV)[10]. Although this virus replicates in most cell lines, it inefficiently killed near-haploid KBM7 cells (Supplementary Fig. 1c). In an unsuccessful attempt to induce pluripotency in KBM7 cells by expression of OCT4 (also called POU5F1), SOX2, MYC and KLF4 (ref. 11), we obtained HAP1 cells (Supplementary Fig. 1a). HAP1 cells grew adherently and no longer expressed haematopoietic markers (Supplementary Fig. 1b). Most of these cells in early passage cultures were haploid for all chromosomes, including chromosome 8 (which is diploid in KBM7 cells). Unlike KBM7 cells, HAP1 cells were susceptible to rVSV-GP-EboV (Supplementary Fig. 1c), allowing screens for filovirus host factors.

We used a retroviral gene-trap vector[9] to mutagenize early-passage HAP1 cells. To generate a control data set, we mapped ~800,000 insertions using deep sequencing (Supplementary Table 1). Next, we selected rVSV-GP-EboV-resistant cells, expanded them as a pool, and mapped insertion sites. Enrichment for mutations in genes was calculated by comparing a gene's mutation frequency in resistant cells to that in the control data set (Supplementary Fig. 2). We identified a set of genes enriched for mutations in the rVSV-GP-EboV-resistant cell population (Fig. 1a, Supplementary Fig. 3 and Supplementary Table 2). Nearly all of these candidate host factors are involved in the architecture and trafficking of endo/lysosomal compartments. Our screen identified cathepsin B (CTSB), the only known host factor for which deletion inhibits Ebola virus entry[5]. Further inspection showed that mutations were highly enriched in genes encoding all six subunits of the HOPS complex (*VPS11*, *VPS16*, *VPS18*, *VPS33A*, *VPS39* and *VPS41*), for which we identified 67 independent mutations. The HOPS complex mediates fusion of endosomes and lysosomes[6] and affects endosome maturation[12,13]. The identification of all members of the HOPS complex demonstrates high, and possibly saturating, coverage of our screen. We also identified factors involved in the biogenesis of endosomes (PIKFYVE, FIG4)[14], lysosomes (BLOC1S1, BLOC1S2)[15], and in targeting of luminal cargo to the endocytic pathway (GNPTAB)[16]. The strongest hit was the Niemann–Pick disease locus *NPC1*, encoding an endo/lysosomal cholesterol transporter[7]. NPC1 also affects endosome/lysosome fusion and fission[17], calcium homeostasis[18] and HIV-1 release[19].

We subcloned the resistant cell population to obtain clones deficient for VPS11, VPS33A and NPC1 (Supplementary Fig. 4a, b and Fig. 1b). These mutants displayed marked resistance to infection by rVSV-GP-EboV and VSV pseudotyped with Ebola virus or Marburg virus GP (Fig. 1c and Supplementary Fig. 4c). Cells lacking a functional HOPS complex or NPC1 were nonetheless fully susceptible to infection by a large panel of other enveloped and non-enveloped viruses, including VSV and recombinant VSV bearing different viral glycoproteins (Fig. 1d and Supplementary Fig. 5). The susceptibility of HAP1 clones to rVSV-GP-EboV infection was restored by expression of the corresponding cDNAs (Supplementary Fig. 6a–c).

Loss of NPC1 causes Niemann–Pick disease, a neurovisceral disorder characterized by cholesterol and sphingolipid accumulation in lysosomes[7]. We tested the susceptibility of patient primary fibroblasts to filovirus-GP-dependent infection. *NPC1*-mutant cells were infected poorly or not at all by rVSV-GP-EboV and VSV pseudotyped with filovirus GP proteins (Fig. 2a, b), and infection was restored by expression of wild-type NPC1 (Fig. 2c).

Mutations in *NPC2* cause identical clinical symptoms and phenocopy defects in lipid transport[20]. Surprisingly, *NPC2*-mutant fibroblasts derived from different patients were susceptible to filovirus-GP-dependent infection (Fig. 2a, b and Supplementary Fig. 7), despite a similar accumulation of cholesterol in *NPC2*- and *NPC1*-mutant cells (Fig. 2a). Moreover, cholesterol clearance from *NPC1*-null cells by cultivation in lipoprotein-depleted growth medium did not confer susceptibility (Supplementary Fig. 8). Therefore, resistance of NPC1-deficient

[1]Whitehead Institute for Biomedical Research, Nine Cambridge Center, Cambridge, Massachusetts 02142, USA. [2]Department of Microbiology and Molecular Genetics, Harvard Medical School, Boston, Massachusetts 02115, USA. [3]Department of Microbiology and Immunology, Albert Einstein College of Medicine, Bronx, New York 10461, USA. [4]US Army Medical Research Institute of Infectious Diseases, 1425 Porter St, Fort Detrick, Maryland 21702-5011, USA. [5]Center for Advanced Molecular Diagnostics, Shapiro 5-058, 70 Francis Street, Boston, Massachusetts 02115, USA. †Present addresses: Department of Microbiology and Immunology, Stanford University School of Medicine, Stanford, California 94304, USA (J.E.C.); Netherlands Cancer Institute, Plesmanlaan 121, 1066 CX Amsterdam, The Netherlands (G.O., T.R.B.).

*These authors contributed equally to this work.

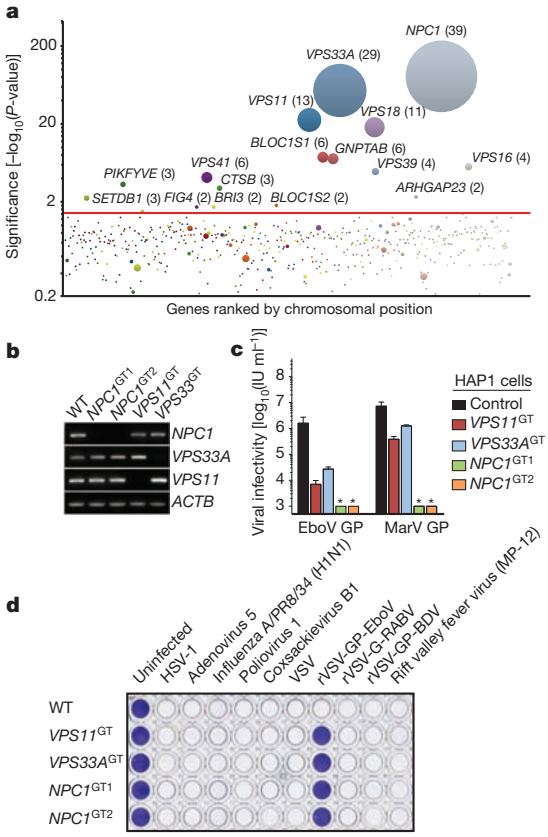

Figure 1 | A haploid genetic screen identifies the HOPS complex and NPC1 as host factors for filovirus entry. **a**, Genes enriched for gene-trap insertions in the rVSV-GP-EboV-selected cell population compared to unselected control cells. Circles represent genes and their size corresponds to the number of independent insertions identified in the rVSV-GP-EboV-selected population. Genes are ranked on the *x*-axis based on chromosomal position. **b**, RT–PCR analysis of the expression levels of *NPC1*, *VPS33A* and *VPS11* in mutant clones. **c**, Infectivity of VSV pseudotyped with the indicated filovirus glycoproteins. IU, infectious units. Means ± standard deviation (s.d.) ($n = 3$) are shown. EboV, Ebola virus (Zaire); MarV, Marburg virus. Asterisk indicates below detection limit. **d**, HAP1 clones were infected with viruses including recombinant VSV viruses carrying rabies or Borna disease virus glycoproteins (rVSV-G-RABV and rVSV-GP-BDV) and stained with crystal violet.

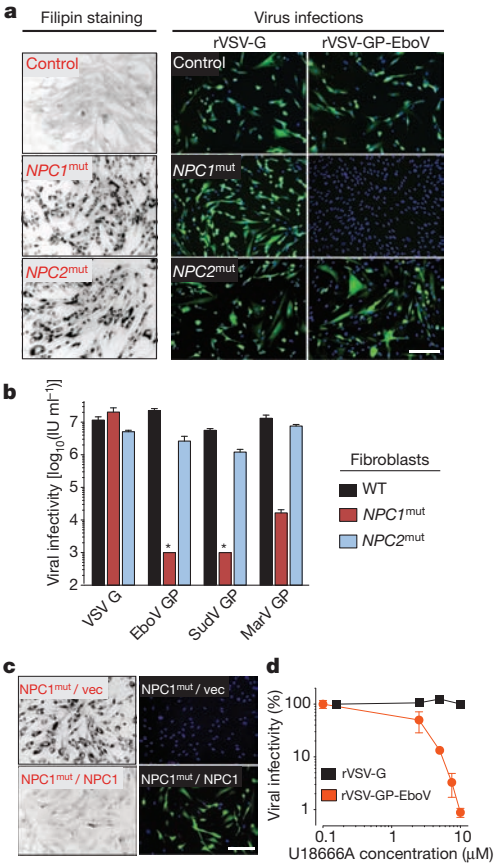

Figure 2 | Viral infection mediated by filovirus glycoproteins requires NPC1 but not NPC2. **a**, Primary skin fibroblasts from a healthy individual and patients carrying homozygous mutations in *NPC1* or *NPC2* were stained with filipin, or challenged with rVSV-G or rVSV-GP-EboV. Filipin-stained (black) and infected cells (green) were visualized by fluorescence microscopy. Filipin-stained images were inverted for clarity. Blue indicates Hoechst nuclear counterstain. **b**, Infectivity of VSV pseudotyped with the indicated viral glycoproteins in control and Niemann–Pick fibroblasts. Asterisk indicates below detection limit. SudV, Sudan virus. **c**, NPC1 patient fibroblasts expressing empty vector or human NPC1 were stained with filipin or challenged with rVSV-GP-EboV. **d**, Infectivity of rVSV-G and rVSV-GP-EboV in Vero cells pre-incubated for 30 min with the indicated concentrations of U18666A. Scale bars, 200 μm (**a**, **c**). Means ± s.d. ($n = 3$–6) are shown (**b**, **d**).

cells to rVSV-GP-EboV is not caused by defects in cholesterol transport per se.

Filoviruses display broad mammalian host and tissue tropism[21,22]. To determine if NPC1 is generally required for filovirus-GP-mediated infection, we used *Npc1*-null Chinese hamster ovary (CHO) cells. Loss of NPC1 conferred complete resistance to viral infection (Supplementary Fig. 6d) that was reversed by expression of human NPC1 (Supplementary Fig. 6e). Certain small molecules such as U18666A (ref. 23) and the antidepressant imipramine[24] cause a cellular phenotype similar to *NPC1* deficiency possibly by targeting NPC1 (ref. 23). Prolonged U18666A treatment has been reported to modestly inhibit VSV[25]. However, we found that brief exposure of Vero cells and HAP1 cells to U18666A or imipramine potently inhibited viral infection mediated by Ebola virus GP but not VSV or rabies virus G (Fig. 2d and Supplementary Figs 9 and 10). Because U18666A inhibits rVSV-GP-EboV infection only when added at early time points, it probably affects entry rather than replication (Supplementary Fig. 10). Thus, NPC1 has a critical role in infection mediated by filovirus glycoproteins that is conserved in mammals and probably independent of NPC1's role in cholesterol transport.

Filoviruses bind to one or more cell-surface molecules[2,26,27] and are internalized by macropinocytosis[28,29]. In *VPS33A*- and *NPC1*-mutant cells, we observed no significant differences in binding or internalization of Alexa-647-labelled rVSV-GP-EboV (Fig. 3a and Supplementary Figs 11 and 12a). Similar results were obtained by flow cytometry using fluorescent Ebola-virus-like particles (Supplementary Fig. 12b). Moreover, bullet-shaped VSV particles were readily observed by electron microscopy at the cell periphery and within plasma membrane invaginations resembling nascent macropinosomes (Fig. 3b). Finally, *VPS33A*- and *NPC1*-null cells were fully susceptible to vaccinia virus entry by macropinocytosis (Supplementary Fig. 13). Thus, GP-mediated entry is not inhibited at viral attachment or early internalization steps in NPC1- or HOPS-defective cells, indicating a downstream defect.

Cathepsin L (CATL; also called CTSL1)-assisted cleavage of Ebola virus GP by CTSB is required for viral membrane fusion[3,5]. Mutant HAP1 cells possess normal CTSB/CATL activity (Supplementary Fig. 14b, c) and were fully susceptible to mammalian reoviruses, which use CTSB or CATL for entry (Supplementary Fig. 14d). Moreover, these cells remained refractory to *in vitro*-cleaved rVSV-GP-EboV particles (Fig. 3c) that no longer required CTSB/CATL activity within Vero cells (Supplementary Fig. 14a). Therefore the HOPS complex and NPC1 are probably required downstream of the initial GP proteolytic processing steps that generate a primed entry intermediate.

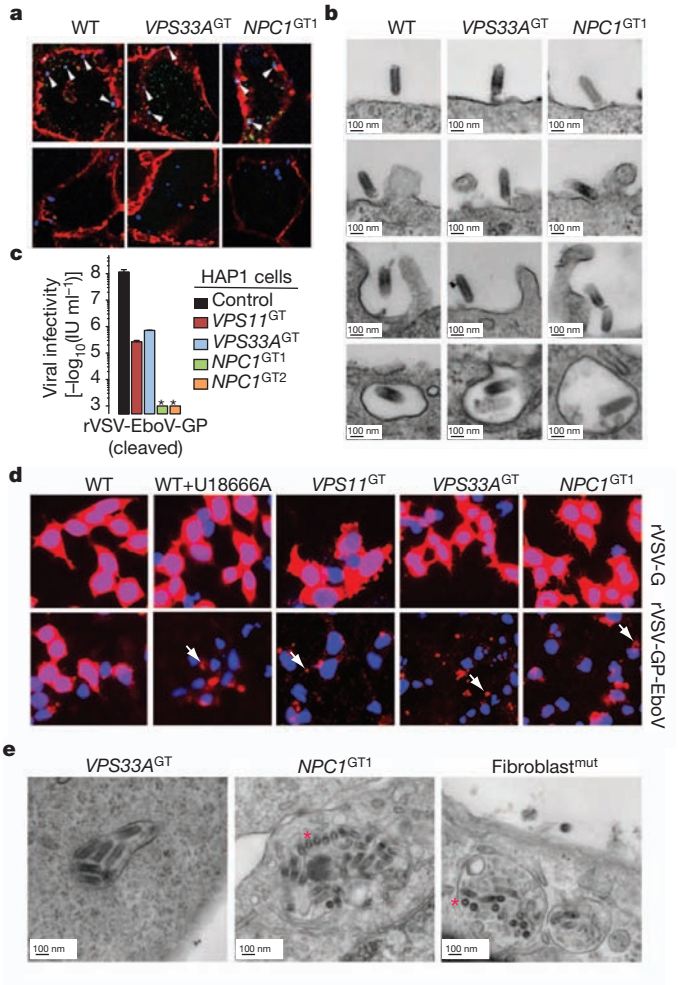

Figure 3 | Virus entry is arrested at a late step in cells deficient for the HOPS complex and NPC1. **a**, Viral particles attach and internalize into HOPS- and NPC1-deficient cells. Indicated HAP1 clones were infected with Alexa-647-labelled rVSV-GP-EboV (blue) at 4 °C. Non-internalized, bound viral particles (arrowheads, blue) were also stained with a GP-specific antibody (green) and the plasma membrane with Alexa-594-wheat germ agglutinin (red) (top panels). To assess viral internalization, cells were heated to 37 °C (bottom panels). Internalized viral particles (blue puncta) are resistant to acid-stripping and inaccessible to a GP antibody. Original magnification, ×63. **b**, Cells were inoculated with rVSV-GP-EboV and examined by transmission electron microscopy. Representative images of early entry steps are shown. **c**, *In vitro*-cleaved rVSV-GP-EboV cannot bypass the infection block observed in *VPS11*^{GT}, *VPS33A*^{GT} and *NPC1*^{GT} cells. GT, gene trap. Infectivity of thermolysin-cleaved rVSV-GP-EboV in the indicated HAP1 clones is shown. Asterisk indicates below the limit of detection. **d**, Viral escape into the cytoplasm is blocked in HOPS-complex- and NPC1-deficient cells. Wild-type HAP1 cells treated with U18666A (10 μg ml^{-1}) and the indicated mutant clones were infected with rVSV-G or rVSV-GP-EboV virus for 3 h and processed for VSV M staining (red). Punctate staining is indicated by arrows. Original magnification, ×20. **e**, Electron micrographs of rVSV-GP-EboV-infected VPS33A- and NPC1-deficient HAP1 cells and NPC1-deficient fibroblasts showing agglomerations of bullet-shaped VSV particles in vesicular compartments. All images were taken at 3 h after inoculation. Asterisks highlight rVSV-GP-EboV particles in cross-section.

Finally, we used the intracellular distribution of the internal VSV M (matrix) protein as a marker for membrane fusion (Fig. 3d). Cells were infected with native VSV or rVSV-GP-EboV and immunostained to visualize the incoming M protein. Endosomal acid-pH-dependent entry of either virus into wild-type HAP1 cells caused redistribution of the incoming viral M throughout the cytoplasm (Fig. 3d and Supplementary Fig. 15a). By contrast, only punctate, perinuclear M staining was obtained in drug-treated and mutant cells infected with rVSV-GP-EboV or rVSV-GP-MarV (Fig. 3d and Supplementary Fig. 15b). Electron micrographs of mutant cells infected with rVSV-GP-EboV revealed agglomerations of viral particles within vesicular compartments (Fig. 3e and Supplementary Fig. 16a) containing LAMP1 (Supplementary Fig. 16b), indicating that fusion and uncoating of incoming virus is arrested. Similarly, U18666A treatment increased the number of viral particles in NPC1- and LAMP1-positive endosomes (Supplementary Fig. 17). Therefore, NPC1 and the HOPS complex are required for late step(s) in filovirus entry leading to viral membrane fusion and escape from the lysosomal compartment.

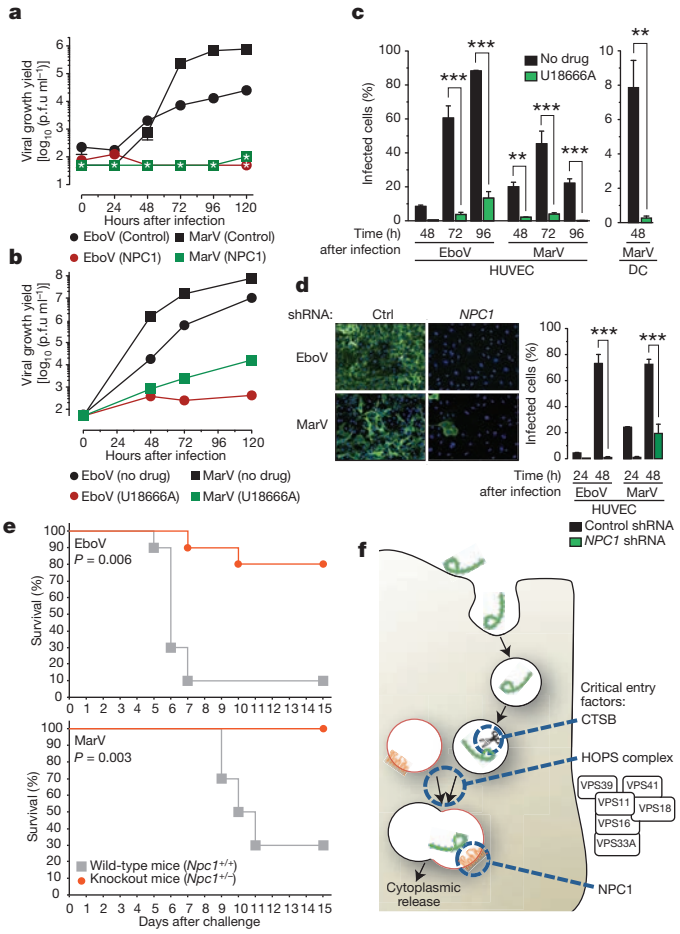

Figure 4 | NPC1 function is required for infection by authentic Ebola and Marburg viruses. **a**, NPC1 patient fibroblasts were exposed to Ebola virus (EboV) or Marburg virus (MarV) at a multiplicity of infection (MOI) of 0.1. Supernatants were harvested and yields of infectious virus were measured. Asterisk indicates below detection limit. p.f.u., plaque-forming units. **b**, Vero cells treated with DMSO or U18666A (20 μM) were infected with Ebola virus or Marburg virus at a MOI of 0.1 and yields of infectious virus were measured. **c**, Human peripheral blood monocyte-derived dendritic cells (DC) and umbilical-vein endothelial cells (HUVEC) were infected in the presence or absence of U18666A at a MOI of 3 and the percentage of infected cells was determined by immunostaining. **d**, HUVECs were transduced with lentiviral vectors expressing a non-targeting short hairpin (sh)RNA (Ctrl) or an shRNA targeting *NPC1*, infected with Ebola virus or Marburg virus at a MOI of 3 and the percentage of infected cells was determined. Representative images of cells 48 h after infection are also shown: green, viral antigen; blue, nuclear counterstain. For panels **a**–**d**, Means ± s.d. are shown ($n = 2$–3). In panels **a**, **b**, error bars are not visible because they are within the symbols. For panels **c**, **d**, $^{**}P < 0.01$; $^{***}P < 0.001$. **e**, Survival of *Npc1*$^{+/+}$ and *Npc1*$^{+/-}$ mice ($n = 10$ for each group) inoculated intraperitoneally with ~1,000 p.f.u. of mouse-adapted Ebola virus or Marburg virus. **f**, A proposed hypothetical model for the roles of CTSB, the HOPS complex and NPC1 in Ebola virus entry.

We next tested if infection by authentic Ebola virus and Marburg virus is affected in *NPC1*-mutant primary patient fibroblasts. Yields of viral progeny were profoundly reduced for both viruses in mutant cells (Fig. 4a). Marked reductions in viral yield were also obtained in Vero cells treated with U18666A (Fig. 4b). Moreover U18666A greatly reduced infection of human peripheral blood monocyte-derived dendritic cells and umbilical-vein endothelial cells (HUVECs) (Fig. 4c), without affecting cell number or morphology (Supplementary Fig. 19). Finally, knockdown of *NPC1* in HUVECs diminished infection by filoviruses (Fig. 4d and Supplementary Fig. 18). These findings indicate that NPC1 is critical for authentic filovirus infection.

We assessed the effect of *NPC1* mutation in lethal mouse models of Ebola virus and Marburg virus infection. Heterozygous *Npc1* ($Npc1^{+/-}$) knockout mice and their wild-type littermates were challenged with mouse-adapted Ebola virus or Marburg virus and monitored for 28 days. Whereas $Npc1^{+/+}$ mice rapidly succumbed to infection with either filovirus, $Npc1^{+/-}$ mice were largely protected (Fig. 4e).

We have used global gene disruption in human cells to discover components of the unusual entry pathway used by filoviruses. Most of the identified genes affect aspects of lysosome function, indicating that filoviruses exploit this organelle differently from all other viruses that we have tested (Fig. 4f). The unanticipated role for the hereditary disease gene *NPC1* in viral entry, infection and pathogenesis may facilitate the development of antifilovirus therapeutics.

METHODS SUMMARY

Adherent HAP1 cells were generated by the introduction of OCT4/SOX2/Myc and KLF4 transcription factors. 100 million cells were mutagenized using a retroviral gene-trap vector. Insertion sites were mapped for approximately 1% of the unselected population using parallel sequencing. Cells were infected with rVSV-GP-EboV and the resistant cell population was expanded. Genes that were statistically enriched for mutation events in the selected population were identified, and the roles of selected genes in filovirus entry were characterized.

Full Methods and any associated references are available in the online version of the paper at www.nature.com/nature.

Received 9 December 2010; accepted 30 June 2011.
Published online 24 August 2011.

1. Feldmann, H. & Geisbert, T. W. Ebola haemorrhagic fever. *Lancet* **377,** 849–862 (2010).
2. Lee, J. E. & Saphire, E. O. Ebolavirus glycoprotein structure and mechanism of entry. *Future Virol.* **4,** 621–635 (2009).
3. Schornberg, K. *et al.* Role of endosomal cathepsins in entry mediated by the Ebola virus glycoprotein. *J. Virol.* **80,** 4174–4178 (2006).
4. Kuhn, J. H. *et al.* Conserved receptor-binding domains of Lake Victoria marburgvirus and Zaire ebolavirus bind a common receptor. *J. Biol. Chem.* **281,** 15951–15958 (2006).
5. Chandran, K., Sullivan, N. J., Felbor, U., Whelan, S. P. & Cunningham, J. M. Endosomal proteolysis of the Ebola virus glycoprotein is necessary for infection. *Science* **308,** 1643–1645 (2005).
6. Nickerson, D. P., Brett, C. L. & Merz, A. J. Vps-C complexes: gatekeepers of endolysosomal traffic. *Curr. Opin. Cell Biol.* **21,** 543–551 (2009).
7. Carstea, E. D. *et al.* Niemann-Pick C1 disease gene: homology to mediators of cholesterol homeostasis. *Science* **277,** 228–231 (1997).
8. Carette, J. E. *et al.* Global gene disruption in human cells to assign genes to phenotypes by deep sequencing. *Nature Biotechnol.* **29,** 542–546 (2011).
9. Carette, J. E. *et al.* Haploid genetic screens in human cells identify host factors used by pathogens. *Science* **326,** 1231–1235 (2009).
10. Wong, A. C., Sandesara, R. G., Mulherkar, N., Whelan, S. P. & Chandran, K. A forward genetic strategy reveals destabilizing mutations in the Ebolavirus glycoprotein that alter its protease dependence during cell entry. *J. Virol.* **84,** 163–175 (2010).
11. Takahashi, K. *et al.* Induction of pluripotent stem cells from adult human fibroblasts by defined factors. *Cell* **131,** 861–872 (2007).
12. Poteryaev, D., Datta, S., Ackema, K., Zerial, M. & Spang, A. Identification of the switch in early-to-late endosome transition. *Cell* **141,** 497–508 (2010).
13. Rink, J., Ghigo, E., Kalaidzidis, Y. & Zerial, M. Rab conversion as a mechanism of progression from early to late endosomes. *Cell* **122,** 735–749 (2005).
14. Sbrissa, D. *et al.* Core protein machinery for mammalian phosphatidylinositol 3,5-bisphosphate synthesis and turnover that regulates the progression of endosomal transport. Novel Sac phosphatase joins the ArPIKfyve-PIKfyve complex. *J. Biol. Chem.* **282,** 23878–23891 (2007).
15. Dell'Angelica, E. C. The building BLOC(k)s of lysosomes and related organelles. *Curr. Opin. Cell Biol.* **16,** 458–464 (2004).
16. Tiede, S. *et al.* Mucolipidosis II is caused by mutations in GNPTA encoding the alpha/beta GlcNAc-1-phosphotransferase. *Nature Med.* **11,** 1109–1112 (2005).
17. Goldman, S. D. & Krise, J. P. Niemann-Pick C1 functions independently of Niemann-Pick C2 in the initial stage of retrograde transport of membrane-impermeable lysosomal cargo. *J. Biol. Chem.* **285,** 4983–4994 (2010).
18. Lloyd-Evans, E. *et al.* Niemann-Pick disease type C1 is a sphingosine storage disease that causes deregulation of lysosomal calcium. *Nature Med.* **14,** 1247–1255 (2008).
19. Tang, Y. Y., Leao, I. C., Coleman, E. M., Broughton, R. S. & Hildreth, J. E. K. Deficiency of Niemann-Pick type C-1 protein impairs release of human immunodeficiency virus type 1 and results in Gag accumulation in late endosomal/lysosomal compartments. *J. Virol.* **83,** 7982–7995 (2009).
20. Naureckiene, S. *et al.* Identification of HE1 as the second gene of Niemann-Pick C disease. *Science* **290,** 2298–2301 (2000).
21. Takada, A. *et al.* A system for functional analysis of Ebola virus glycoprotein. *Proc. Natl Acad. Sci. USA* **94,** 14764–14769 (1997).
22. Wool-Lewis, R. J. & Bates, P. Characterization of Ebola virus entry by using pseudotyped viruses: identification of receptor-deficient cell lines. *J. Virol.* **72,** 3155–3160 (1998).
23. Cenedella, R. J. Cholesterol synthesis inhibitor U18666A and the role of sterol metabolism and trafficking in numerous pathophysiological processes. *Lipids* **44,** 477–487 (2009).
24. Rodriguez-Lafrasse, C. *et al.* Abnormal cholesterol metabolism in imipramine-treated fibroblast cultures. Similarities with Niemann-Pick type C disease. *Biochim Biophys Acta* **1043,** 123–128 (1990).
25. Sobo, K. *et al.* Late endosomal cholesterol accumulation leads to impaired intra-endosomal trafficking. *Plos One* **2,** e851 (2007).
26. Kondratowicz, A. S. *et al.* T-cell immunoglobulin and mucin domain 1 (TIM-1) is a receptor for Zaire Ebolavirus and Lake Victoria Marburgvirus. *Proc. Natl Acad. Sci. USA.* **108,** 8426–8431 (2011).
27. Alvarez, C. P. *et al.* C-type lectins DC-SIGN and L-SIGN mediate cellular entry by Ebola virus *in cis* and *in trans*. *J. Virol.* **76,** 6841–6844 (2002).
28. Saeed, M. F., Kolokoltsov, A. A., Albrecht, T. & Davey, R. A. Cellular entry of ebola virus involves uptake by a macropinocytosis-like mechanism and subsequent trafficking through early and late endosomes. *PLoS Pathog.* **6,** http://dx.doi.org/10.1371/journal.ppat.1001110 (2010).
29. Nanbo, A. *et al.* Ebolavirus is internalized into host cells via macropinocytosis in a viral glycoprotein-dependent manner. *PLoS Pathog.* **6,** http://dx.doi.org/10.1371/journal.ppat.1001121 (2010).

Supplementary Information is linked to the online version of the paper at www.nature.com/nature.

Acknowledgements We would like to thank M. Kielian, H. Ploegh, V. Prasad and D. Sabatini for critical reading of the manuscript and valuable advice; C. Guimaraes, V. Blomen and T. Peterson for suggestions; M. Bogyo for providing the CTSB/CATL activity probe (GB111); T.-Y. Chang for the gift of NPC1-null CHO cells; D. Lyles for the antibody to VSV M; M. Nibert for providing reovirus; J. de la Torre for providing rVSV-GP-BDV; J. Wojcechowskyj for providing RVF; E. Mühlberger for providing Ebola cDNA; and M. Ericsson for support with electron microscopy. This research was supported by NIH grants R01 AI088027 (K.C.), AI081842 and U54 AI057159 (NERCE-BEID) (S.P.W.), and R21 HG004938 (T.R.B.), and by the DTRA Project, CBM.VAXPLAT.05.10.RD.005 (J.M.D.). T.R.B. was additionally supported by the Whitehead Fellows Program. S.P.W. is a recipient of a Burroughs Wellcome Investigators in the Pathogenesis of Infectious Disease Award. A.C.W. was additionally supported by NIH-funded training programs T32 GM007288 and T32 AI070117 at the Albert Einstein College of Medicine. Opinions, interpretations, conclusions and recommendations are those of the authors and are not necessarily endorsed by the US Army.

Author Contributions K.C., S.P.W., T.R.B. and J.M.D. were the senior authors of this study and made equivalent contributions. The study was conceived by K.C., S.P.W. and T.R.B. J.E.C. and T.R.B. devised and implemented the haploid genetic screen, generated the HAP1 cells and identified hits by deep sequencing and cell cloning. P.D.C. carried out karyotype analysis on the HAP1 line. K.C. created and characterized the rVSV-GP-EboV virus used in the screen. A.M.G. created the rVSV-G-RABV. J.E.C., G.O. and K.C. performed entry and infection experiments with the HAP1 cells. A.C.W. and K.C. carried out entry and infection experiments with rVSVs in human fibroblasts, CHO and Vero cells. N.M. and K.C. carried out RNAi experiments with primary cells. M.R. was involved in experimental strategy and design and performed entry and infection experiments by high-resolution fluorescence and electron microscopy. N.M. carried out VLP entry experiments and P.J.K., the replicon assay. A.C.W. performed the cysteine cathepsin enzyme assays. A.S.H., A.I.K. and J.M.D. performed the infection and animal challenge experiments with the authentic viral agents. G.R. performed fluorescence microscopy and image analysis with filovirus-infected cell cultures. J.E.C., K.C., S.P.W. and T.R.B. wrote the paper.

Author Information Reprints and permissions information is available at www.nature.com/reprints. The authors declare competing financial interests: details accompany the full-text HTML version of the paper at www.nature.com/nature. Readers are welcome to comment on the online version of this article at www.nature.com/nature. Correspondence and requests for materials should be addressed to T.R.B. (t.brummelkamp@nki.nl), K.C. (kartik.chandran@einstein.yu.edu), S.P.W. (sean_whelan@hms.harvard.edu) or J.M.D. (John.M.Dye1@us.army.mil).

METHODS

Cells. KBM7 cells and derivatives were maintained in IMDM supplemented with 10% FCS, L-glutamine, and penicillin–streptomycin. Vero cells and primary human dermal fibroblasts (Coriell Institute for Medical Research) were maintained in DMEM supplemented with 10% FCS, L-glutamine and penicillin–streptomycin. Wild-type and NPC1-null (CT43) Chinese hamster ovary (CHO) fibroblasts were maintained in DMEM-Ham's F-12 medium (50-50 mix) supplemented with 10% FCS, L-glutamine and penicillin–streptomycin[30].

To generate dendritic cells, primary human monocytes were cultured at 37 °C, 5% CO_2, and 80% humidity in RPMI supplemented with 10% human serum, L-glutamine, sodium pyruvate, HEPES, penicillin–streptomycin, recombinant human granulocyte monocyte-colony stimulating factor (50 ng ml^{-1}) and recombinant human interleukin-4 (50 ng ml^{-1}) for 6 days. Cytokines were added every 2 days by replacing half of the culture volume with fresh culture media. Dendritic cells were collected on day 6, characterized by flow cytometry (see below) and used immediately. Human umbilical vein endothelial cells (HUVECs) were obtained from Lonza and maintained in endothelial grown medium (EGM; Lonza).

HAP1 cells were used for the haploid screen and fibroblasts or CHO cells were used for hit validation and functional studies. Vero cells are commonly used in studies of filovirus replication, because they are highly susceptible to infection. Dendritic cell and HUVECs resemble cell types that are early and late targets of filovirus infection *in vivo*, respectively[31,32].

Flow cytometry of dendritic cells. Human dendritic cells were treated with Fc-block (BD Pharmingen) before incubation with mouse anti-human CD11c-APC (BioLegend) and mouse anti-human CD209-PE or isotype controls. Dendritic cells were washed and re-suspended in PBS for flow cytometric analysis using a BD FACSCanto II flow cytometer (BD Biosciences). Data analysis was completed using FlowJo software. >95% of cells were routinely observed to be CD11c$^+$, DC-SIGN$^+$.

Viruses. Recombinant VSV expressing eGFP and Ebola virus GP (rVSV-GP-EboV) was recovered and amplified as described[10]. Recombinant rVSV-GP-BDV was provided by J. C. de la Torre. rVSV-G-RABV was generated by replacement of the VSV G ORF in VSV-eGFP[33] with that of the SAD-B19 strain of rabies virus, and recombinant virus was recovered and amplified[34]. VSV pseudotypes bearing glycoproteins derived from Ebola virus, Sudan virus and Marburg virus were generated as described[35].

The following non-recombinant viruses were used: adenovirus type 5 (ATCC), coxsackievirus B1 (ATCC), poliovirus 1 Mahoney (provided by C. Schlieker), HSV-1 KOS (provided by H. Ploegh), influenza A/PR8/34 (H1N1) (Charles Rivers), Rift valley fever virus MP-12 (provided by J. Wojcechowskyj), and mammalian reovirus serotype 1 (provided by M. Nibert).

Generation of HAP1 cells. Retroviruses encoding SOX2, MYC, OCT4 and KLF4 were produced[36]. Concentrated virus was used to infect near-haploid KBM7 cells in three consecutive rounds of spin-infection with an interval of 12 h. Colonies were picked and tested for ploidy. One clonally derived cell line (referred to as HAP1) was further grown and characterized. Karyotyping analysis demonstrated that most cells (27 of 39) were fully haploid, a smaller population (9 of 39) was haploid for all chromosomes except chromosome 8, like the parental KBM7 cells. Less than 10% (3 of 39) was diploid for all chromosomes except for chromosome 8, which was tetraploid.

Haploid genetic screen. Gene-trap virus was produced in 293T cells by transfection of pGT-GFP, pGT-GFP+1 and pGT-GFP+2 combined with pAdvantage, CMV-VSVG and Gag-pol. The virus was concentrated using ultracentrifugation for 1.5 h at 25,000 r.p.m. in a Beckman SW28 rotor. 100 million HAP1 cells were infected. A proportion of the cells was harvested for genomic DNA isolation to create a control data set. For the screen, 100 million mutagenized cells were exposed to rVSV-GP-EboV at a MOI ~100. The resistant colonies were expanded and ~30 million cells were used for genomic DNA isolation.

Sequence analysis of gene-trap insertion sites. Insertion sites were identified by sequencing the genomic DNA flanking gene-trap proviral DNA as described before[8]. In short, a control data set was generated containing insertion sites in mutagenized HAP1 cells before selection with rVSV-GP-EboV. Genomic DNA was isolated from ~40 million cells and subjected to a linear PCR followed by linker ligation, PCR and sequencing using the Genome Analyser platform (Illumina). Insertion sites were mapped to the human genome and insertion sites were identified that were located in Refseq genes. Insertions in this control data set comprise ~400,000 independent insertions that meet this criteria (Supplementary Table 1). To generate the experimental data set, insertions in the mutagenized HAP1 cells after selection with rVSV-GP-EboV were identified using an inverse PCR protocol followed by sequencing using the Genome Analyser. The number of inactivating mutations (that is, sense orientation or present in exon) per individual gene was counted as well as the total number of inactivating insertions for all genes. Enrichment of a gene in the screen was calculated by comparing how often that gene was mutated in the screen compared to how often the gene carries an insertion in the control data set. For each gene a *P*-value (corrected for false discovery rate) was calculated using the one-sided Fisher exact test (Supplementary Table 2).

Characterization of the HAP1 mutant lines. Genomic DNA was isolated using Qiamp DNA mini kit (Qiagen). To confirm that the cells were truly clonal and to confirm the absence of the wild-type DNA locus, a PCR was performed with primers flanking the insertion site using the following primers: (NPC-F1, 5′-GAAGTTGGTCTGGCGATGGAG-3′; NPC1-R2, 5′-AAGGTCCTGATCTAAAACTCTAG-3′; VPS33A-F1, 5′-TGTCCTACGGCCGAGTGAACC-3′; VPS33A-R1, 5′-CTGTACACTTTGCTCAGTTTCC-3′; VPS11-F1, 5′-GAAGGAGCCGCTGAGCAATGATG-3′; VPS11-R1, 5′-GGCCAGAATTTAGTAGCAGCAAC-3′). To confirm the correct insertion of the gene trap at the different loci a PCR was performed using the reverse (R1) primers of *NPC1*, *VPS11* and *VPS33A* combined with a primer specific for the gene trap vector: PGT-F1; 5′-TCTCCAAATCTCGGTGGAAC-3′. To determine RNA expression levels of *NPC1*, *VPS11* and *VPS33A*, total RNA was reverse transcribed using Superscript III (Invitrogen) and amplified using gene-specific primers: *VPS11*, 5′-CTGCTTCCAAGTTCCTTTGC-3′ and 5′-AAGATTCGAGTGCAGAGTGG-3′; *NPC1*, 5′-CCACAGCATGACCGCTC-3′ and 5′-CAGCTCACAAAACAGGTTCAG-3′; *VPS33A*, 5′-TTAACACCTCTTGCCACTCAG-3′ and 5′-TGTGTCTTTCCTCGAATGCTG-3′.

Generation of stable cell populations expressing an NPC1–Flag fusion protein. A human cDNA encoding NPC1 (Origene) was ligated in-frame to a triple Flag sequence and the resulting gene encoding a C-terminally Flag-tagged NPC1 protein was subcloned into the pBABE-puro retroviral vector[37]. Retroviral particles packaging the NPC1–Flag gene or no insert were generated by triple transfection in 293T cells, and used to infect control and NPC1-deficient human fibroblasts and CHO lines. Puromycin-resistant stable cell populations were generated.

Cell viability assays for virus treatments. KBM7 and HAP1 cells were seeded at 10,000 cells per well in 96-well tissue culture plates and treated with the indicated concentrations of rVSV-GP-EboV. After 3 days cell viability was measured using an XTT colorimetric assay (Roche). Viability is plotted as percentage viability compared to untreated control. To compare susceptibility of the HAP1 mutants to different viruses, they were seeded at 10,000 cells per well and treated with different cytolytic viruses at a concentration that in pilot experiments was the lowest concentration to produce extensive cytopathic effects. Three days after treatment, viable, adherent cells were fixed with 4% formaldehyde in phosphate-buffered saline (PBS) and stained with crystal violet.

VSV infectivity measurements. Infectivities of VSV pseudotypes were measured by manual counting of eGFP-positive cells using fluorescence microscopy at 16–26 h after infection, as described previously[5]. rVSV-GP-EboV infectivity was measured by fluorescent-focus assay (FFA), as described previously[10].

Filipin staining. Filipin staining to visualize intracellular cholesterol was done as described[38]. Cells were fixed with paraformaldehyde (3%) for 15 min at 25° C. After three PBS washes, cells were incubated with filipin complex from *Streptomyces filipinensis* (Sigma-Aldrich) (50 μg ml^{-1}) in the dark for 1 h at room temperature. After three PBS washes, cells were visualized by fluorescence microscopy in the DAPI channel.

Measurements of cysteine cathepsin activity. Enzymatic activities of CTSB and CATL in acidified post-nuclear extracts of Vero cells, human fibroblasts and CHO lines were assayed with fluorogenic peptide substrates Z-Arg-Arg-AMC (Bachem Inc.) and (Z-Phe-Arg)2-R110 (Invitrogen) as described[39]. As a control for assay specificity, enzyme activities were also assessed in extracts pre-treated with E-64 (10 μM), a broad-spectrum cysteine protease inhibitor, as previously described[10]. Active CTSB and CATL within intact cells were labelled with the fluorescently labelled activity-based probe GB111 (1 μM) and visualized by gel electrophoresis and fluorimaging, as described previously[40].

Purification and dye conjugation of rVSV-GP-EboV. rVSV-GP-EboV was purified and labelled with Alexa Fluor 647 (Molecular Probes, Invitrogen Corporation) as described[41] with minor modifications. Briefly, Alexa Fluor 647 (Molecular Probes, Invitrogen Corporation) was solubilized in DMSO at 10 mg ml^{-1} and incubated at a concentration of 31.25 μg ml^{-1} with purified rVSV-GP-EboV (0.5 mg ml^{-1}) in 0.1 M $NaHCO_3$ (pH 8.3) for 90 min at room temperature. Virus was separated from free dye by ultracentrifugation. Labelled viruses were re-suspended in NTE (10 mM Tris pH 7.4, 100 mM NaCl, 1 mM EDTA) and stored at −80 °C.

Virus binding/internalization assay. Cells were inoculated with a MOI of 200–500 of Alexa-647-labelled rVSV-GP-EboV at 4 °C for 30 min to allow binding of virus to the cell surface. Cells were subsequently fixed in 2% paraformaldehyde (to examine virus binding) or after a 2-h incubation at 37 °C and an acid wash to remove surface-bound virus. The cellular plasma membrane was labelled by incubation of

cells with 1 μg ml^{-1} Alexa Fluor 594 wheat germ agglutinin (Molecular Probes, Invitrogen) in PBS for 15 min at room temperature. External virus particles were detected using a 1:2,000 dilution of antibody 265.1, a mouse monoclonal antibody specific for Ebola GP. The GP antibodies were detected by Alexa-488-conjugated goat anti-mouse secondary antibody (Molecular Probes, Invitrogen). After washing with PBS, cells were mounted onto glass slides using Prolong Antifade Reagent (Invitrogen, Molecular Probes). Fluorescence was monitored with an epifluorescence microscope (Axiovert 200M; Carl Zeiss) equipped with a ×63 objective and representative images were acquired using Slidebook 4.2 software (Intelligent Imaging Innovations)[41,42].

VSV M protein-release assay. Cells grown on 12-mm coverslips coated with poly-D-lysine (Sigma-Aldrich) were pre-treated with 5 μg ml^{-1} puromycin for 30 min and inoculated with rVSV at a MOI of 200–500 in the presence of puromycin. After 3 h, cells were washed once with PBS and fixed with 2% paraformaldehyde in PBS for 15 min at room temperature. To detect VSV M protein, fixed cells were incubated with a 1:7,500 dilution of monoclonal antibody 23H12 (gift of D. Lyles[43]) in PBS containing 1% BSA and 0.1% Triton X-100 for 30 min at room temperature. Cells were washed three times with PBS, and the anti-M antibodies were detected using a 1:750 dilution of Alexa 594-conjugated goat anti-mouse secondary antibodies. Cells were counter-stained with DAPI to visualize nuclei. Cells were washed three times and mounted onto glass slides after which M localization images were acquired using a Nikon TE2000-U inverted epifluorescence microscope (Nikon Instruments) equipped with a ×20 objective. Representative images were acquired with Metamorph software (Molecular Devices).

Electron microscopy. Confluent cell monolayers in 6-well plates were inoculated with rVSV-GP-EboV at a MOI of 200–500 for 3 h. Cells were fixed for at least 1 h at room temperature in a mixture of 2.5% glutaraldehyde, 1.25% paraformaldehyde and 0.03% picric acid in 0.1 M sodium cacodylate buffer (pH 7.4). Samples were washed extensively in 0.1 M sodium cacodylate buffer (pH 7.4) and treated with 1% osmiumtetroxide and 1.5% potassiumferrocyanide in water for 30 min at room temperature. Treated samples were washed in water, stained in 1% aqueous uranyl acetate for 30 min, and dehydrated in grades of alcohol (70%, 90%, 2× 100%) for 5 min each. Cells were removed from the dish with propyleneoxide and pelleted at 3,000 r.p.m. for 3 min. Samples were infiltrated with Epon mixed with propyleneoxide (1:1) for 2 h at room temperature. Samples were embedded in fresh Epon and left to polymerize for 24–48 h at 65 °C. Ultrathin sections (about 60–80 nm) were cut on a Reichert Ultracut-S microtome and placed onto copper grids. For preparation of cryosections the virus-inoculated cells were rinsed once with PBS and removed from the dish with 0.5 mM EDTA in PBS. The cell suspension was layered on top of an 8% paraformaldehyde cushion in an Eppendorf tube and pelleted for 3 min at 3,000 r.p.m. The supernatant was removed and fresh 4% paraformaldehyde was added. After 2 h incubation, the fixative was replaced with PBS. Before freezing in liquid nitrogen the cell pellets were infiltrated with 2.3 M sucrose in PBS for 15 min. Frozen samples were sectioned at −120 °C and transferred to formvar-carbon-coated copper grids. Grids were stained for lysosomes with a mouse monoclonal antibody raised against LAMP1 (H4A3; Santa Cruz Biotechnology). The LAMP1 antibodies were visualized with Protein-A gold secondary antibodies. Contrasting/embedding of the labelled grids was carried out on ice in 0.3% uranyl acetate in 2% methyl cellulose. All grids were examined in a TecnaiG^2 Spirit BioTWIN mission electron microscope and images were recorded with an AMT 2k CCD camera.

Authentic filoviruses and infections. Vero cells were pre-treated with culture medium lacking or containing U18666A (20 μM) for 1 h at 37 °C. VERO cells and primary human dermal fibroblasts were exposed to Ebola virus Zaire 1995 or Marburg virus Ci67 at a MOI of 0.1 for 1 h. Viral inoculum was removed and fresh culture media with or without drug was added. Samples of culture supernatants were collected and stored at −80 °C until plaque assays were completed.

Dendritic cells were collected and seeded in 96-well poly-D-lysine-coated black plates (Greiner Bio-One) at 5×10^4 cells per well or in 6-well plates at 10^6 cells per well in culture media and incubated overnight at 37 °C. They were pre-treated with medium lacking or containing U18666A as described above. Dendritic cells were exposed to Ebola virus Zaire 1995 or Marburg virus Ci67 at a MOI of 3 for 1 h. Virus inoculum was removed and fresh culture media with or without drug was added. Uninfected cells with or without drug served as negative controls. Cells were incubated at 37 °C and fixed with 10% formalin at designated times. HUVECs were seeded in 96-well poly-D-lysine-coated black plates at 5×10^4 cells per well in culture media, treated with U18666A, infected, and processed as described above for dendritic cells.

Cytotoxicity analysis. Dendritic cells and HUVECs were seeded in 96-well plates. After overnight incubation at 37 °C, U18666A was added at the same concentrations used for the viral infection studies. Cells in culture media without drug served as the untreated control. At indicated times after treatment, an equal volume of CellTiter-Glo Reagent (Promega) was added to wells containing cells in culture media. Luminescence was measured using a plate reader.

Plaque assays for titration of filoviruses. Tenfold serial dilutions of culture supernatants or serum were prepared in modified Eagle's medium with Earle's balanced salts and nonessential amino acids (EMEM/NEAA) plus 5% heat-inactivated fetal bovine serum. Each dilution was inoculated into a well of a 6-well plate containing confluent monolayers of Vero 76 cells. After adsorption for 1 h at 37 °C, monolayers were overlaid with a mixture of 1 part of 1% agarose (Seakem) and 1 part of 2× Eagle basal medium (EBME), 30 mM HEPES buffer and 5% heat-inactivated fetal bovine serum. After incubation at 37 °C, 5% CO_2, 80% humidity for 6 days, a second overlay with 5% Neutral red was added. Plaques were counted the following day, and titres were expressed as p.f.u. ml^{-1}.

Analysis of filovirus-infected cultures by immunofluorescence. Formalin-fixed cells were blocked with 1% bovine serum albumin solution before incubation with primary antibodies. Ebola-virus-infected cells and uninfected controls were incubated with Ebola virus GP-specific monoclonal antibodies 13F6 (ref. 44) or KZ52 (ref. 45). Marburg-virus-infected cells and uninfected controls were incubated with Marburg virus GP-specific monoclonal antibody 9G4. Cells were washed with PBS before incubation with either goat anti-mouse IgG or goat anti-human IgG conjugated to Alexa 488. Cells were counterstained with Hoechst stain (Molecular Probes), washed with PBS and stored at 4 °C.

Image analysis. Images were acquired at 9 fields per well with a ×10 objective lens on a Discovery-1 high content imager (Molecular Devices) or at 6 fields per well with a ×20 objective lens on an Operetta (Perkin Elmer) high content device. Discovery-1 images were analysed with the 'live/dead' module in MetaXpress software. Operetta images were analysed with a customized scheme built from image analysis functions present in Harmony software.

Animals and filovirus challenge experiments. Mouse-adapted Ebola virus has been described[46]. Mouse-adapted Marburg virus Ci67 was provided by S. Bavari[47]. Female and male BALB/c *Npc1*$^{+/-}$ mice and BALB/c *Npc1*$^{+/+}$ mice (5–8-week-old) were obtained from Jackson Laboratory. Mice were housed under specific pathogen-free conditions. Research was conducted in compliance with the Animal Welfare Act and other federal statutes and regulations relating to animals and experiments involving animals and adhered to principles stated in the Guide for the Care and Use of Laboratory Animals (National Research Council, 1996). The facility where this research was conducted is fully accredited by the Association for the Assessment and Accreditation of Laboratory Animal Care International. For infection, mice were inoculated intraperitoneally with a target dose of 1,000 p.f.u. (30,000× the 50% lethal dose) of mouse-adapted Ebola virus or mouse-adapted Marburg Ci67 virus in a biosafety level 4 laboratory. Mice were observed for 28 days after challenge by study personnel and by an impartial third party. Daily observations included evaluation of mice for clinical symptoms such as reduced grooming, ruffled fur, hunched posture, subdued response to stimulation, nasal discharge and bleeding. Serum was collected from surviving mice to confirm virus clearance. Back titration of the challenge dose by plaque assay determined that Ebola-virus-infected mice received 900 p.f.u. per mouse and Marburg-virus-infected mice received 700 p.f.u. per mouse.

RNA interference. Lentiviral vectors expressing an shRNA specific for *NPC1* (Sigma-Aldrich; clone# TRCN0000005428; sequence CCACAAGTTCTATAC CATATT) or a non-targeting control shRNA (Sigma-Aldrich; SHC002; sequence CAACAAGATGAAGAGCACCAA) were packaged into HIV-1 pseudotype virus by transfection in HEK 293T cells and lentivirus-containing supernatants were harvested at 36 h and 48 h after transfection and centrifuged onto HUVECs in 12-well plates in the presence of 6 μg ml^{-1} polybrene at 2,500 r.p.m., 25 °C for 90 min. HepG2 cells were transduced as above but without the centrifugation step. Cells were subjected to puromycin selection 24 h after the last lentiviral transduction (HepG2, 1 μg ml^{-1}; HUVECs, 1.5 μg ml^{-1}) for 48–72 h before harvest for experiments. The level of NPC1 knockdown was assessed by SDS-polyacrylamide gel electrophoresis of cell extracts and immunoblotting with an anti-NPC1 polyclonal antibody (Abcam).

Ebola virus replicon assay. Ebola virus support plasmids were created by cloning the *NP*, *VP35*, *VP30* and *L* genes from cDNA (provided by E. Mühlberger[48]) into pGEM3 (Promega) and the mutant pL-D742A plasmid was generated by QuikChange site-directed mutagenesis (Stratagene). Truncated versions of the Ebola virus non-coding sequence were generated by overlap-extension PCR and appended to the *eGFP* ORF. The replicon pZEm was prepared as described previously[49]. The replicon RNA sequence is flanked on the 5′ end by a truncated T7 promoter with a single guanosine nucleotide and on the 3′ end by the HDV ribozyme sequence and T7 terminator. The transcribed replicon RNA consists of the following EboV Zaire sequences (GenBank accession AF086833): [5′]-single guanosine nucleotide–176-nucleotide genomic 5′ terminus–55-nucleotide *L* mRNA 3′ UTR–*eGFP* ORF (antisense orientation)–100-nucleotide *NP* mRNA 5′ UTR–155-nucleotide genomic 3′ terminus-[3′]. The viral replicon

assay was performed as described previously[49] except that U18666A (20 μg ml^{-1}) was included in the supplemented DMEM where indicated. Images were collected directly from 6-cm dishes with a Zeiss Axioplan inverted fluorescent microscope.

30. Cruz, J. C., Sugii, S., Yu, C. & Chang, T. Y. Role of Niemann-Pick type C1 protein in intracellular trafficking of low density lipoprotein-derived cholesterol. *J. Biol. Chem.* **275,** 4013–4021 (2000).
31. Geisbert, T. W. *et al.* Pathogenesis of Ebola hemorrhagic fever in cynomolgus macaques: evidence that dendritic cells are early and sustained targets of infection. *Am. J. Pathol.* **163,** 2347–2370 (2003).
32. Geisbert, T. W. *et al.* Pathogenesis of Ebola hemorrhagic fever in primate models: evidence that hemorrhage is not a direct effect of virus-induced cytolysis of endothelial cells. *Am. J. Pathol.* **163,** 2371–2382 (2003).
33. Whelan, S. P., Barr, J. N. & Wertz, G. W. Identification of a minimal size requirement for termination of vesicular stomatitis virus mRNA: implications for the mechanism of transcription. *J. Virol.* **74,** 8268–8276 (2000).
34. Whelan, S. P., Ball, L. A., Barr, J. N. & Wertz, G. T. Efficient recovery of infectious vesicular stomatitis virus entirely from cDNA clones. *Proc. Natl Acad. Sci. USA* **92,** 8388–8392 (1995).
35. Takada, A., Watanabe, S., Okazaki, K., Kida, H. & Kawaoka, Y. Infectivity-enhancing antibodies to Ebola virus glycoprotein. *J. Virol.* **75,** 2324–2330 (2001).
36. Carette, J. E. *et al.* Generation of iPSCs from cultured human malignant cells. *Blood* **115,** 4039–4042 (2010).
37. Morgenstern, J. P. & Land, H. Advanced mammalian gene transfer: high titre retroviral vectors with multiple drug selection markers and a complementary helper-free packaging cell line. *Nucleic Acids Res.* **18,** 3587–3596 (1990).
38. Pentchev, P. G. *et al.* The cholesterol storage disorder of the mutant BALB/c mouse. A primary genetic lesion closely linked to defective esterification of exogenously derived cholesterol and its relationship to human type C Niemann-Pick disease. *J. Biol. Chem.* **261,** 2772–2777 (1986).
39. Ebert, D. H., Deussing, J., Peters, C. & Dermody, T. S. Cathepsin L and cathepsin B mediate reovirus disassembly in murine fibroblast cells. *J. Biol. Chem.* **277,** 24609–24617 (2002).
40. Blum, G. *et al.* Dynamic imaging of protease activity with fluorescently quenched activity-based probes. *Nature Chem. Biol.* **1,** 203–209 (2005).
41. Cureton, D. K., Massol, R. H., Saffarian, S., Kirchhausen, T. L. & Whelan, S. P. Vesicular stomatitis virus enters cells through vesicles incompletely coated with clathrin that depend upon actin for internalization. *PLoS Pathog.* **5,** e1000394 (2009).
42. Ehrlich, M. *et al.* Endocytosis by random initiation and stabilization of clathrin-coated pits. *Cell* **118,** 591–605 (2004).
43. Lefrancois, L. & Lyles, D. S. The interaction of antibody with the major surface glycoprotein of vesicular stomatitis virus. I. Analysis of neutralizing epitopes with monoclonal antibodies. *Virology* **121,** 157–167 (1982).
44. Wilson, J. A. *et al.* Epitopes involved in antibody-mediated protection from Ebola virus. *Science* **287,** 1664–1666 (2000).
45. Maruyama, T. *et al.* Ebola virus can be effectively neutralized by antibody produced in natural human infection. *J. Virol.* **73,** 6024–6030 (1999).
46. Bray, M., Davis, K., Geisbert, T., Schmaljohn, C. & Huggins, J. A mouse model for evaluation of prophylaxis and therapy of Ebola hemorrhagic fever. *J. Infect. Dis.* **178,** 651–661 (1998).
47. Warfield, K. L. *et al.* Development of a model for marburgvirus based on severe-combined immunodeficiency mice. *Virol. J.* **4,** 108 (2007).
48. Muhlberger, E., Weik, M., Volchkov, V. E., Klenk, H. D. & Becker, S. Comparison of the transcription and replication strategies of Marburg virus and Ebola virus by using artificial replication systems. *J. Virol.* **73,** 2333–2342 (1999).
49. Kranzusch, P. J. *et al.* Assembly of a functional Machupo virus polymerase complex. *Proc. Natl Acad Sci USA* **107,** 20069–20074 (2010).

doi:10.1038/nature10348

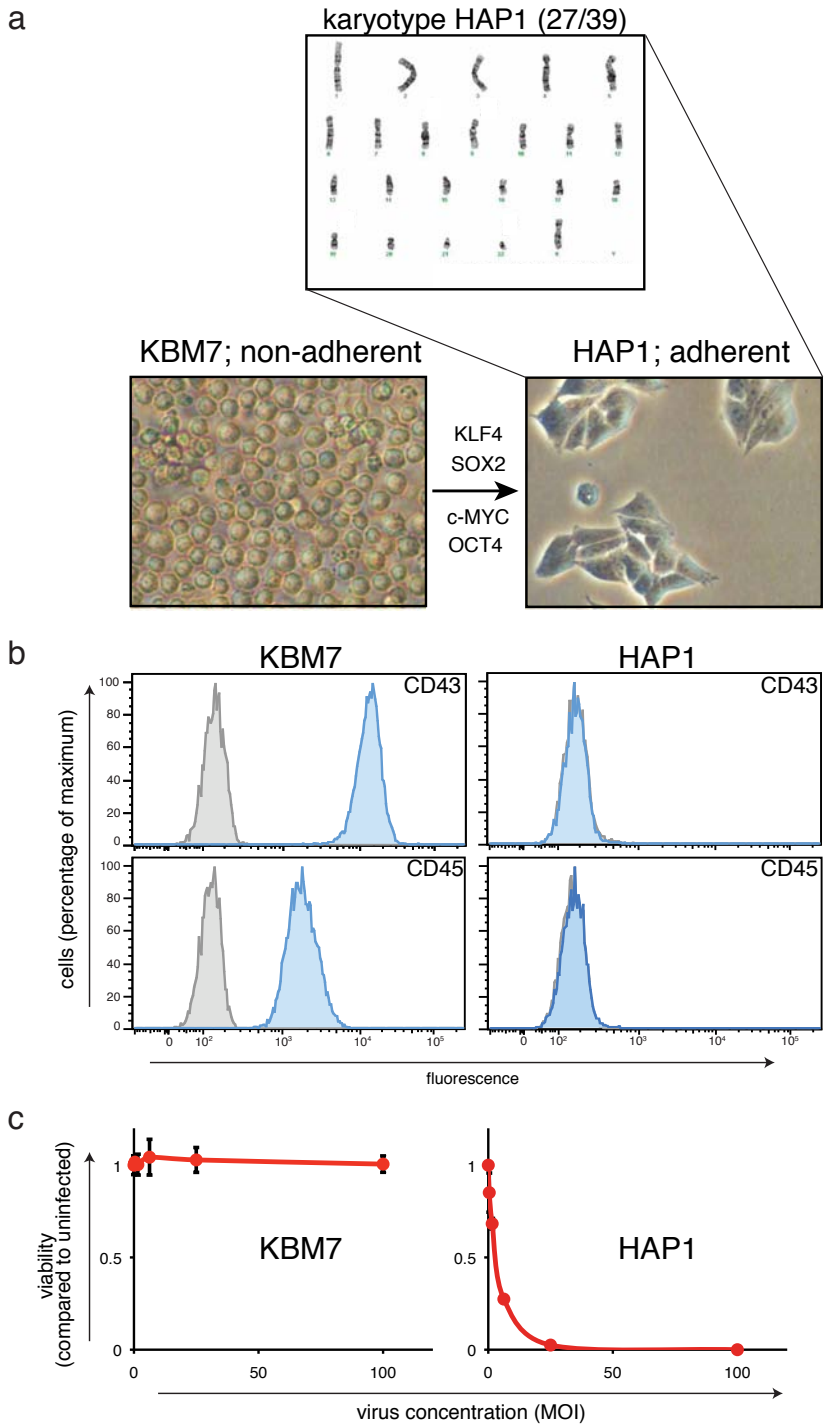

Supplemental Figure 1. Generation of HAP1 cells and susceptibility to rVSV-GP-EboV. **a**, Near-haploid KBM7 cells were coinfected with retroviral vectors expressing OCT4/ SOX2/c-MYC and KLF4 and an adherently growing subclone was identified (HAP1 cells). Karyotypic analysis of HAP1 cells indicates that the majority of cells (27 out of 39 analyzed) is haploid for all chromosomes **b**, Staining of KBM7 cells and HAP1 cells with pan-hematopoietic markers CD43 and CD45. Stained cells were examined by flow-cytometry. The unstained control is indicated in grey. **c**. Susceptibility of HAP1 and KBM7 cells to cell-killing by rVSV-GP-EboV.

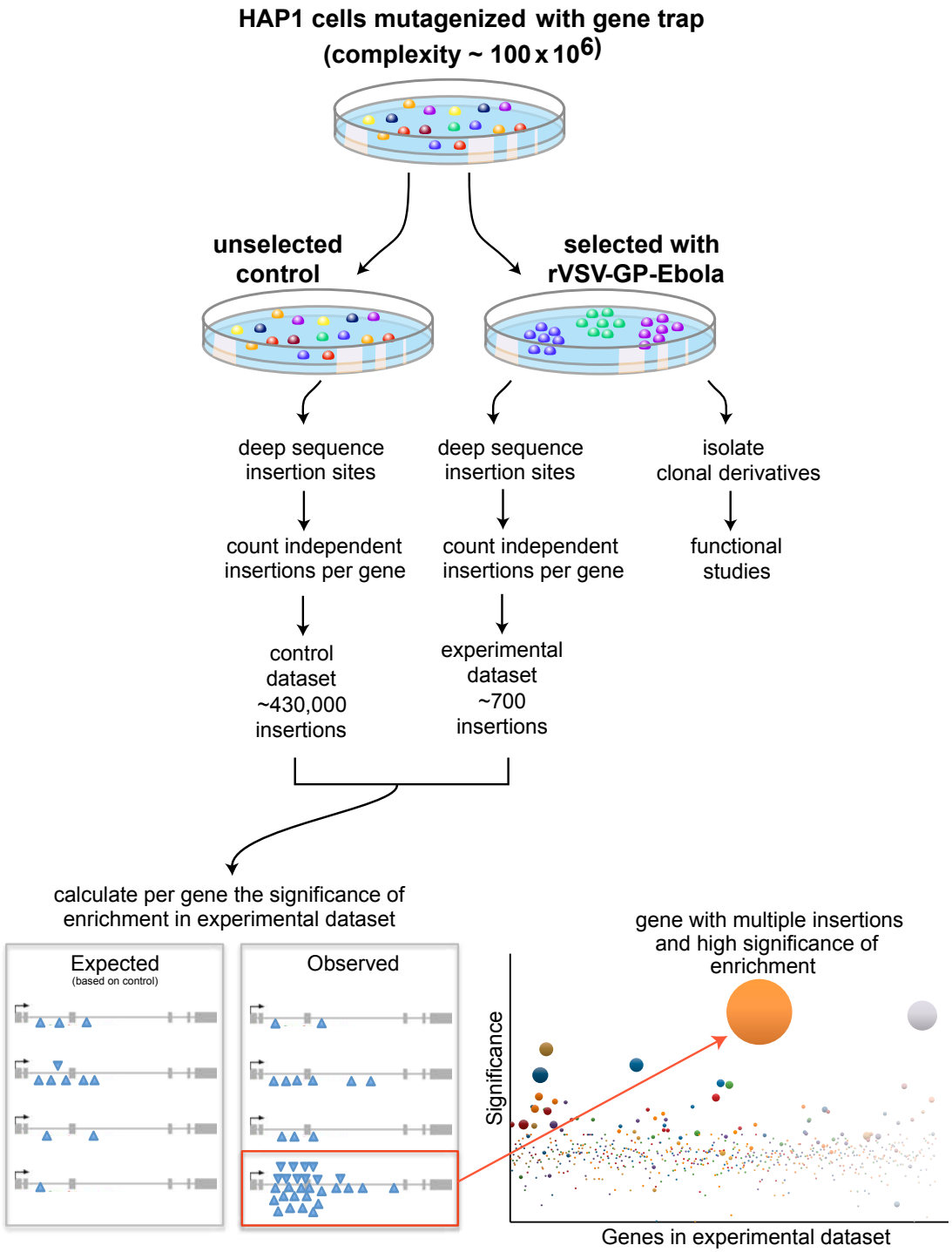

Supplemental Figure 2. Outline of the haploid genetic screen to identify host factors for Ebola virus entry. 100 million early passage HAP1 cells were infected with gene-trap virus and further expanded. A subset of cells was used to characterize the distribution of gene-trap insertion across the human genome. Sequences flanking the gene-traps were amplified, sequenced in parallel and aligned to the human genome. Independent insertion events into annotated genes were counted. 100 million cells were infected with rVSV-GP-EboV virus and resistant clones were pooled and expanded. Most of these cells were used to amplify sequences flanking the gene-traps, sequence the insertion sites in parallel, and align these sequences to the human genome. A subset of the cells was used to obtain NPC1^{GT} and VPS33^{GT} cells through subcloning. Gene disruption events in the selected population were compared to the unselected cell population and genes that were significantly enriched for mutations were identified.

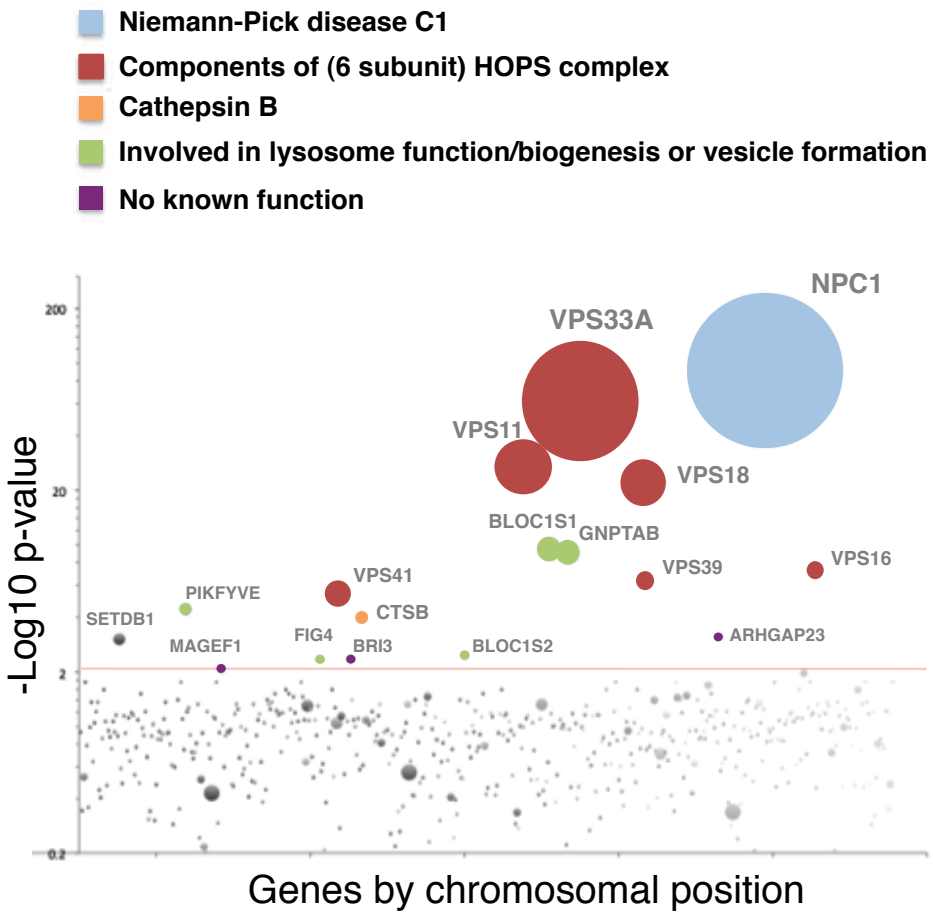

Supplemental Figure 3. Classes of genes that are required for rVSV-GP-EboV induced cytotoxicity. Significant hits were labeled according to the following annotation: Niemann-Pick disease C1, lysosomal cholesterol transporter (blue), component of 6-subunit HOPS complex (red), cathepsin B (orange), involved in lysosome function /biogenesis (green) or having no known function (purple).

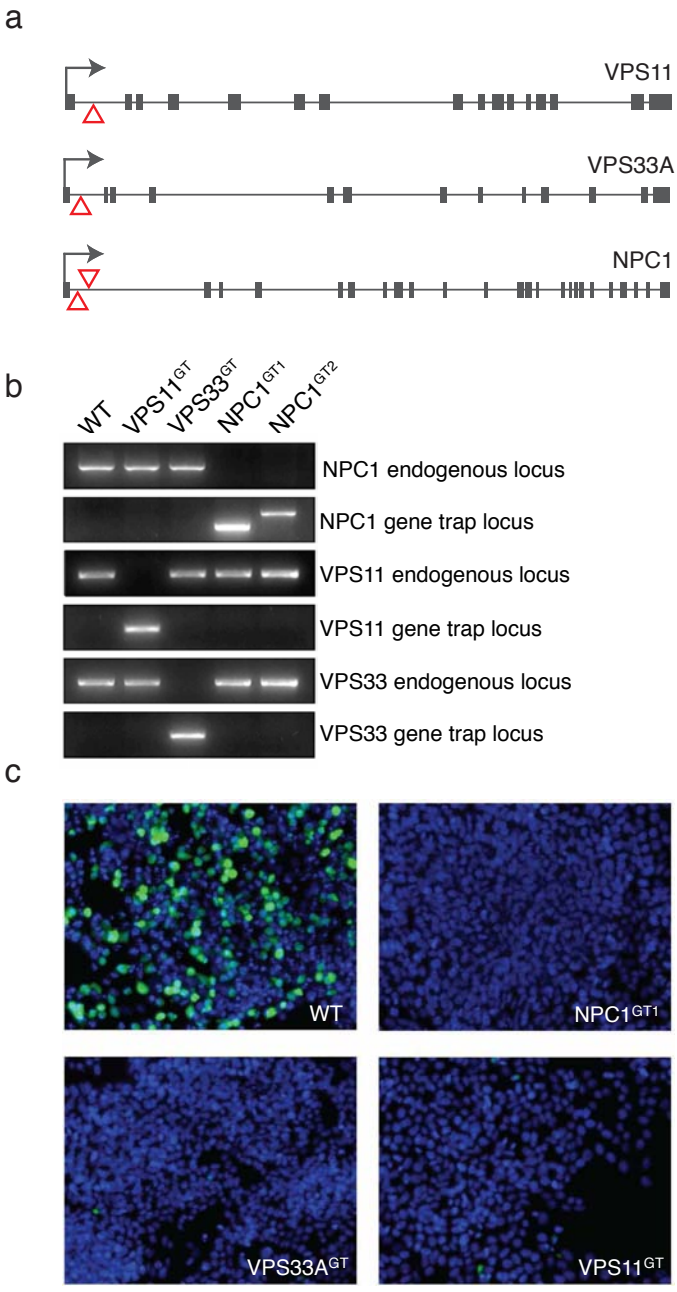

Supplemental Figure 4. Identification and characterization of HAP1 cells carrying gene-trap insertions in the NPC1, VPS11 and VPS33A loci. **a**, Schematic outline of the positions of gene-trap insertions in the corresponding genes. Gene-traps were located in the sense orientation in intronic sequences of the 5'-end of the gene and are therefore predicted to disrupt gene function. **b**, Clonal cell lines carrying the gene-trap insertions in the corresponding loci were identified through subcloning. Genotyping indicates the absence of wild type genomic loci and the presence of gene-trap loci. **c**, Cells carrying gene-trap insertions in the corresponding loci and wild type HAP1 cells were inoculated with rVSV-GP-EboV, and infected cells (green) were visualized by fluorescence microscopy 12 h later.

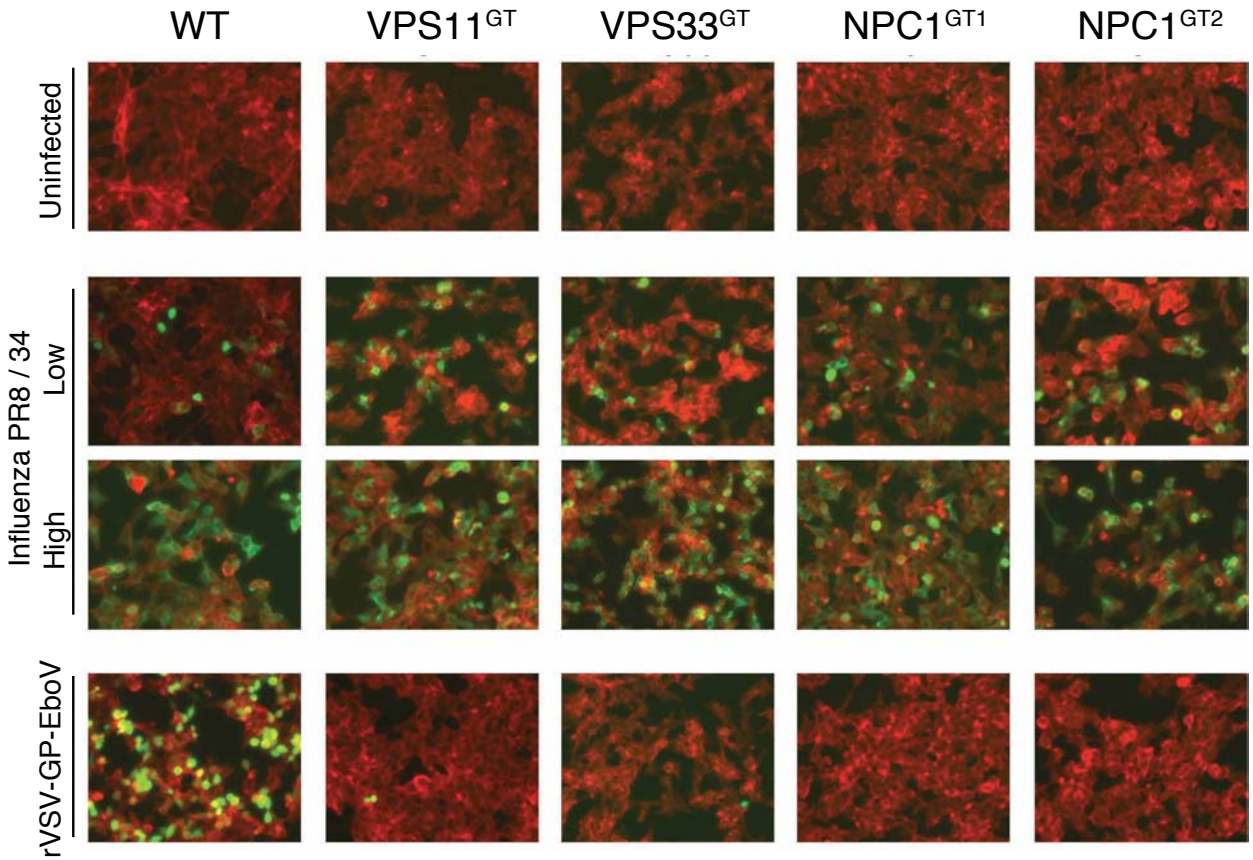

Supplemental Figure 5. Susceptibility of NPC1 and HOPS mutant cell lines to influenza A virus infection. Cells were infected with influenza A/PR8/34 virus (two different MOIs), or VSV-GP-EboV. Influenza virus-infected cells (green) were stained 11 h later with antibodies directed against the viral nucleoprotein and visualized by fluorescence microscopy. rVSV-GP-EboV-infected cells (green) were imaged by eGFP fluorescence. Cells were counterstained with a β-actin-specific antibody (red).

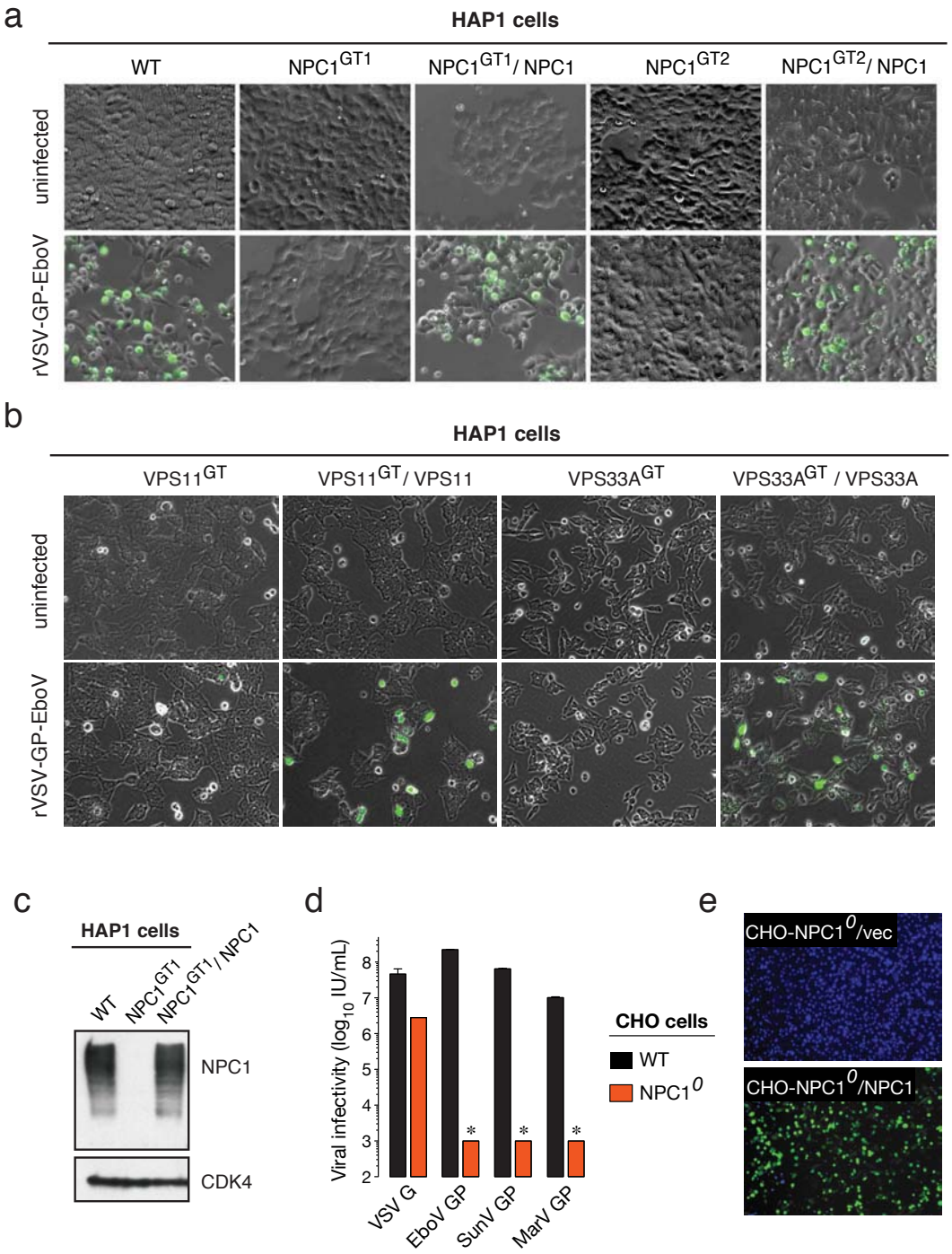

Supplemental Figure 6. Loss of NPC1, VPS11, or VPS33A confers resistance to viral infection mediated by the Ebola virus glycoprotein that can be restored by exogenous expression of the respective host gene. **a**, HAP1 cells carrying independent gene-trap insertions in the NPC1 locus were infected with a retroviral vector directing the expression of NPC1, or with a control virus. Cells were then infected with rVSV-GP-EboV, and eGFP-positive infected cells (green) were visualized 12 h later by fluorescence microscopy. Overlaid differential-interference contrast (DIC) and fluorescence micrographs of the same fields are shown. **b**, HAP1 cells carrying gene-trap insertions in the VPS11 and VPS33A locus were infected with a retroviral vector directing the expression of the corresponding cDNAs, or with a control virus. Cells were treated as in panel a. **c**, Immunoblot blot analysis of NPC1 in HAP1 cells, HAP1 cells carrying a gene-trap insertion in the NPC1 locus and the same cell line infected with the NPC1-expressing retrovirus. CDK4 was used a loading control. **d**, Wild type or NPC1-deficient CHO cells were challenged with VSV pseudotyped with the indicated viral glycoproteins, and viral infectivity was measured 24 h later. **e**, NPC1-deficient CHO cells were infected with a retroviral vector directing the expression of NPC1, or with a control virus. Cells were then infected with rVSV-GP-EboV, and eGFP-positive infected cells were visualized by fluorescence microscopy 14 h later.

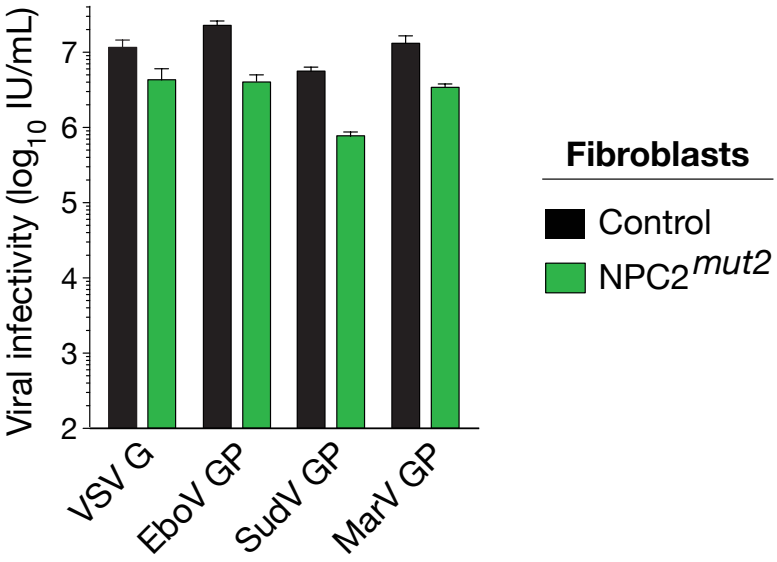

Supplemental Figure 7. NPC2-mutant fibroblasts derived from a second Niemann-Pick patient are susceptible to viral infection mediated by the Ebola virus glycoprotein. Fibroblasts from an apparently normal individual and a Niemann-Pick patient carrying homozygous mutations in NPC2 were infected with VSV pseudotypes bearing the indicated viral glycoproteins, and viral infectivity was measured 24 h later. Means ± standard deviation (SD) are shown.

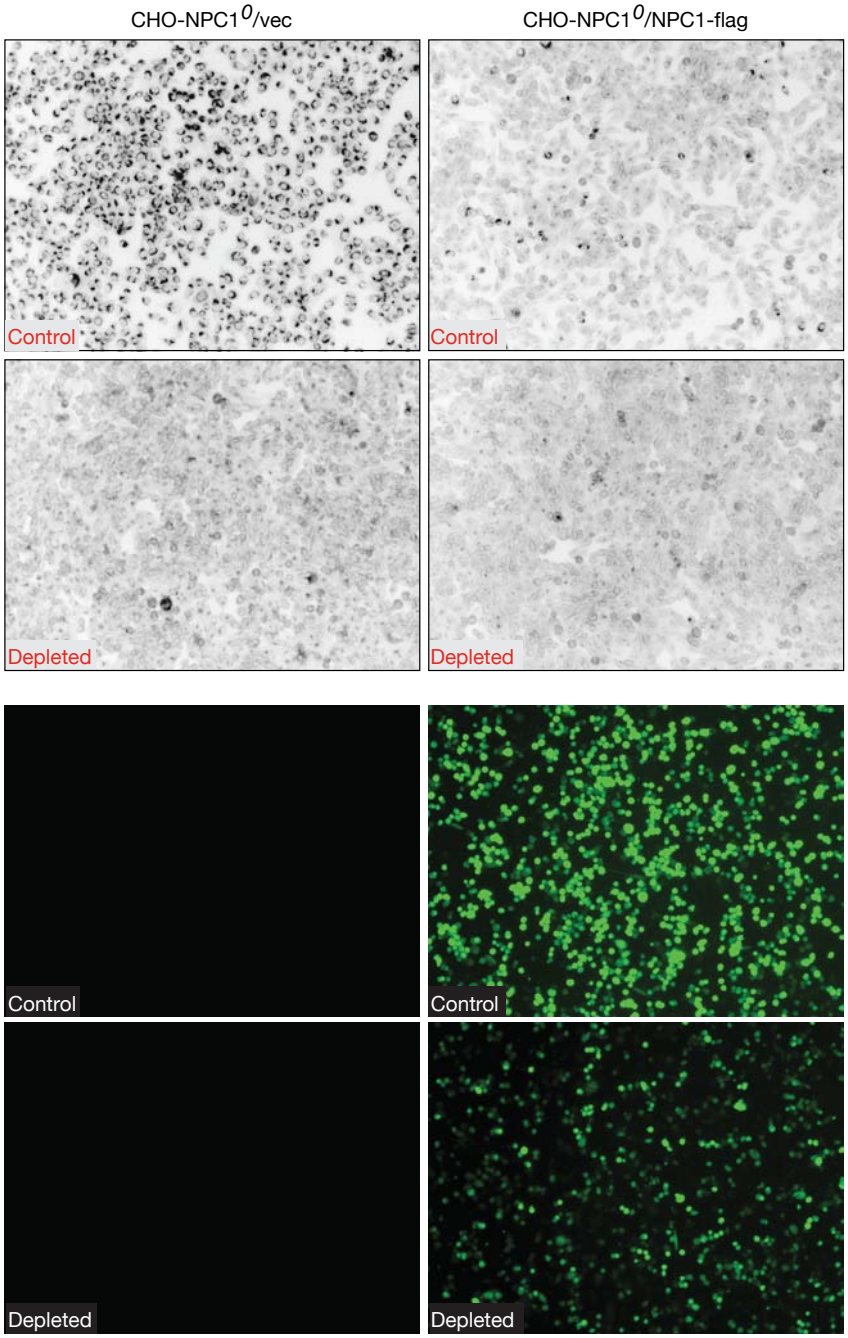

Supplemental Figure 8. Clearance of accumulated cholesterol does not render NPC1-deficient cells susceptible to infection by rVSV-GP-EboV. Wild type and NPC1-null CHO cells were cultivated either in normal growth medium (control) or in growth medium containing lipoprotein-depleted fetal bovine serum for 6 days. Cells were then stained with filipin to visualize accumulated cholesterol (top panels) or infected with rVSV-GP-EboV (bottom panels). Filipin-stained (black) or infected cells (green) were visualized by fluorescence microscopy.

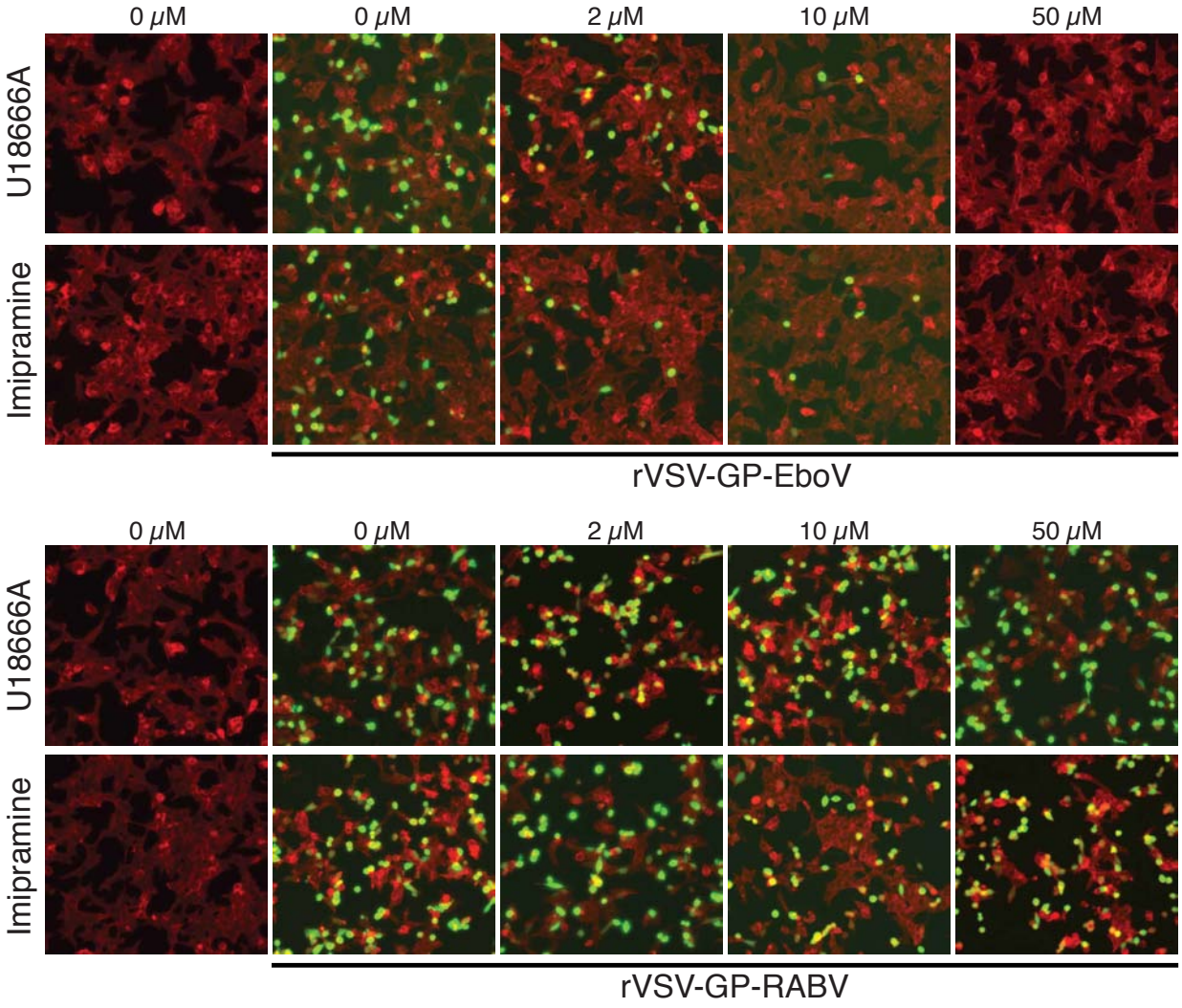

Supplemental Figure 9. Viral infection mediated by the Ebola glycoprotein is inhibited by imipramine and U18666A. HAP1 cells were pretreated for 30 minutes with the indicated concentrations of U18666A or the anti-depressant imipramine and then infected with rVSV-GP-EboV or rVSV-G-RABV carrying a GFP transgene. eGFP-positive infected cells were visualized by fluorescence microscopy 8 h later. Cells were counterstained with β-actin (red).

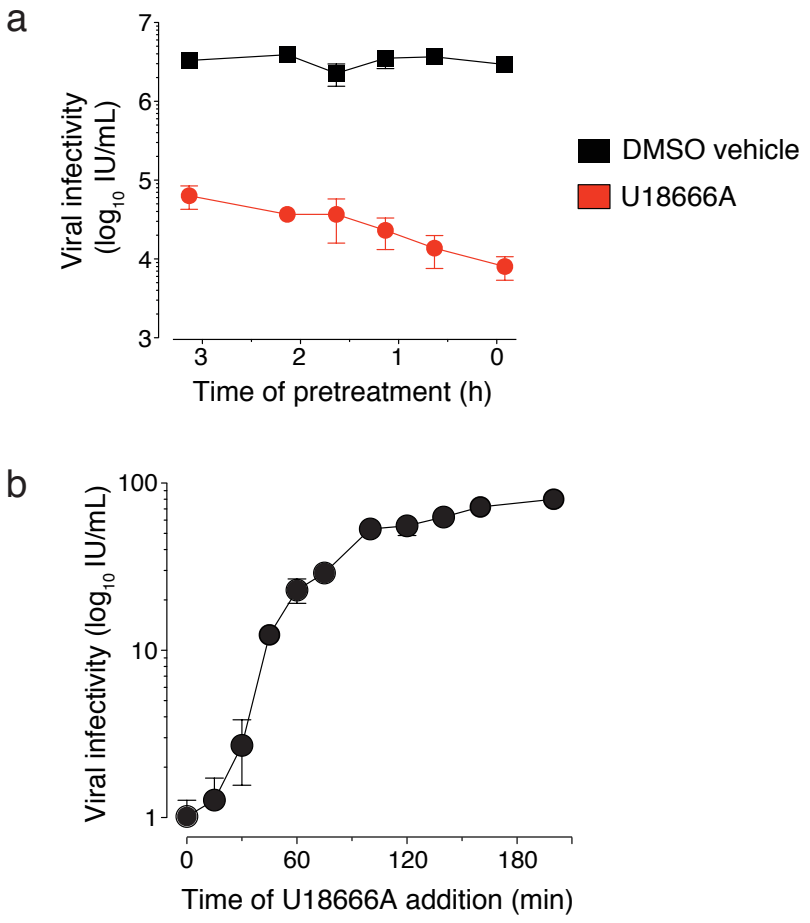

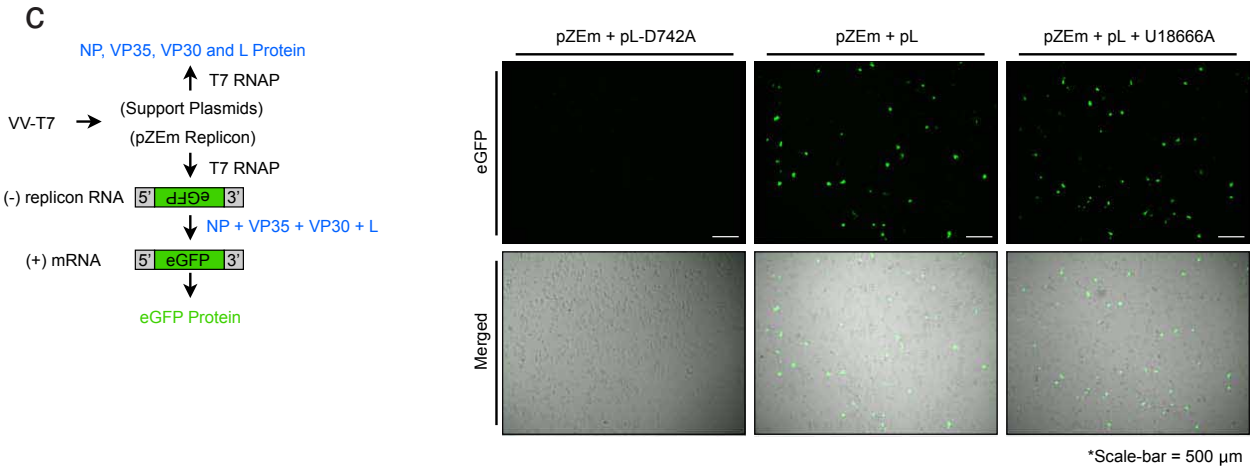

Supplemental Figure 10. U18666A acts rapidly to inhibit Ebola virus GP-dependent entry and does not affect the cytoplasmic steps of Ebola viral replication. **a**, Vero cells were left untreated or were pretreated with U18666A (20 µM) for the indicated times and then infected with rVSV-GP-EboV in the presence of U18666A. After 1 h, viral entry was terminated by addition of NH4Cl (20 mM). Viral infectivity was measured 12-14 h later. **b**, Vero cells were exposed to VSV-GP-EboV virus for 1 h at 4˚C, washed to remove unbound inoculum, and then incubated in growth medium at 37˚C. At the indicated times post-warming, growth medium containing U18666A (20 µM final) was added. Viral infectivity was measured 16 h later. Means ± standard deviation (SD) are shown. **c**, T7 RNA polymerase drives the production of the Ebola virus replication proteins (NP, VP35, VP30 and L) from individual plasmids with T7 promoters. Additionally, T7 RNAP produces a negative-sense viral genome analogue RNA from the replicon plasmid (pZEm) that encodes eGFP. The viral polymerase machinery utilizes the replicon RNA as a transcription template to produce a positive-sense eGFP mRNA resulting in eGFP protein production. A single amino-acid substitution to the active site of the RdRP domain within L abolishes replicon activity and eGFP production and serves as negative control.

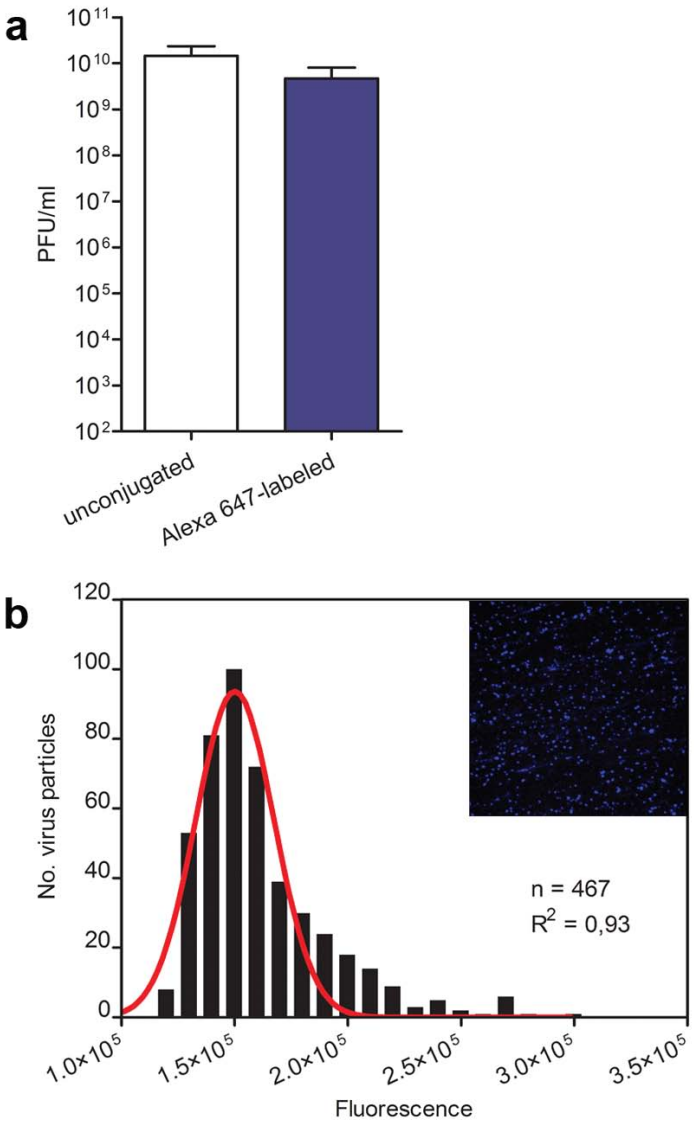

Supplemental Figure 11. Alexa Fluor 647 conjugation to rVSV-GP-EboV particles does not affect infectivity. **a**, rVSV-GP-EboV titers following Alexa 647 conjugation as determined by plaque assay. Means ± standard deviation (SD) are shown (n = 3). **b**, Net fluorescence intensity of Alexa 647-labeled rVSV-GP-EboV particles. Virions on a glass coverslip were imaged by confocal fluorescence microscopy, and the fluorescence intensity (arbitrary units) of each particle was measured. The distribution of particle fluorescence intensities is depicted as a histogram plot in which the red line shows the best-fit Gaussian curve. The inset shows a representative image of virus particles (blue).

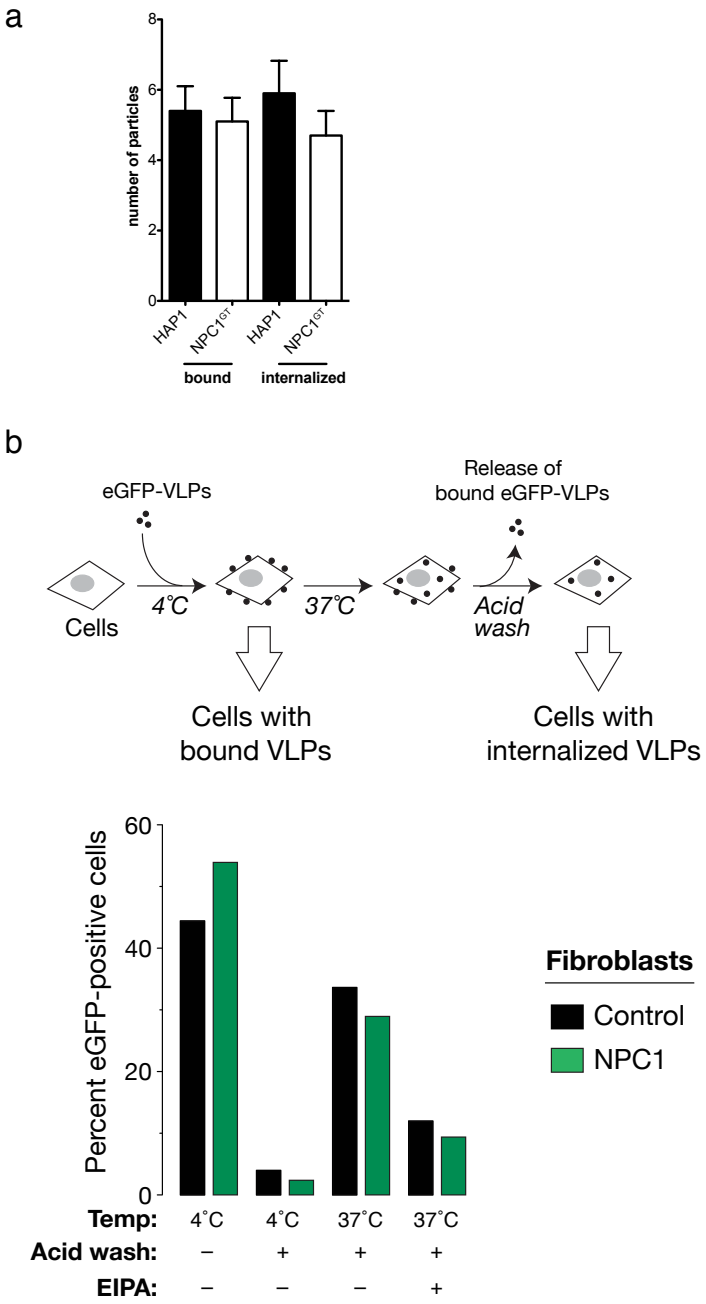

Supplemental Figure 12. Quantification of viral attachment and internalization in NPC1-deficient HAP1 cells and NPC1-mutant fibroblasts. **a**, Ten individual cells of the experiment described in the legend of Figure 3A were used for quantification of bound/internalized viral particles. Briefly, the indicated HAP1 clones were infected with Alexa 647-labeled rVSV-GP-EboV at 4°C. Non-internalized, bound viral particles were stained with a GP-specific antibody. Internalization of virus was assessed by warming cells to 37°C for 2 h. Cells were counterstained with Alexa 594-wheat germ agglutinin to outline the plasma membrane. Viral particles were counted using Slidebook 4.2 software (Intelligent Imaging Innovations; Denver, CO). **b**, Virus-like particles (VLPs) containing the EboV matrix protein VP40 fused to the enhanced green fluorescent protein (eGFP-VP40) were generated as described previously. Binding and internalization of VLPs in control and NPC1-mutant fibroblasts was assessed as follows. Cells were exposed to VLPs (1–2 μg protein/well) by centrifugation at 250 x g and 4˚C for 1 h, washed with PBS, and fixed with paraformaldehyde (PFA). The degree of VLP binding (eGFP signal sensitive to a brief acid wash at pH 3.0) was quantitated by flow cytometry. To allow viral internalization, some samples were shifted to 37˚C for 3 h after the 4˚C step, and then washed and fixed as described above. The degree of VLP internalization (eGFP signal resistant to a brief acid wash at pH 3.0) was quantitated by flow cytometry. VLP internalization into control and NPC1-mutant fibroblasts was sensitive to preincubation of cells with EIPA (50 μM), as observed in other cell types. Averages of two trials from a representative experiment are shown.

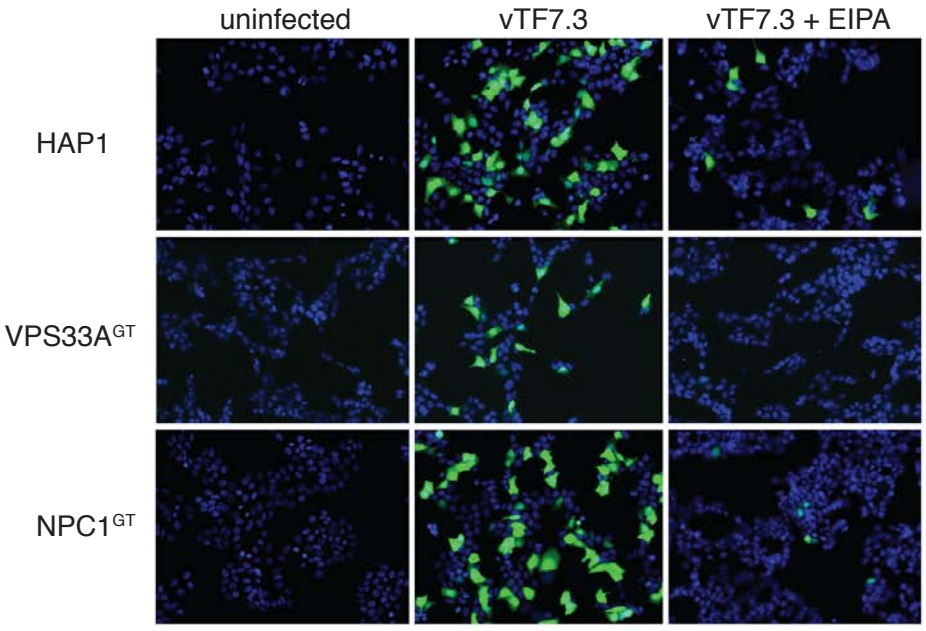

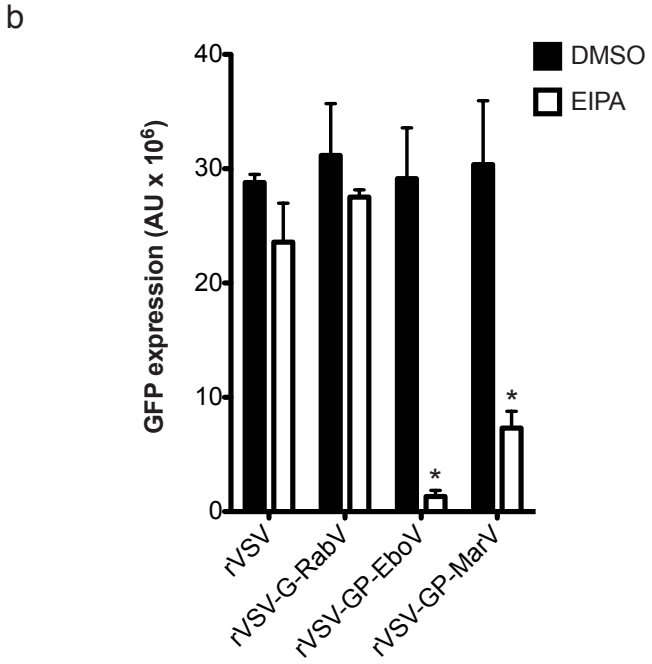

Supplemental Figure 13. HOPS- and NPC1-deficient cells support entry of vaccinia virus, which is internalized by macropinocytosis. **a**, The indicated HAP1 clones were inoculated with a vaccinia virus expressing T7 polymerase (vTF7.3) for 1 h at 37°C in PBS in the absence or presence of 50 μM EIPA. As a control, cells were inoculated with PBS alone. Subsequently, all cells were transfected with a plasmid encoding GFP (green) under control of a T7 promoter. 4 h after transfection cells were fixed with 4% PFA at RT and the nuclei were stained with DAPI (blue). Fluorescence images were acquired and representative images are indicated. **b**, HAP1 cells were challenged with the indicated viruses (MOI 10) in the absence or presence of 50 μM EIPA. GFP expression was quantified 8 h post inoculation by using a Typhoon 9400 Fluorescent Imager (GE Healthcare). The data are presented in arbitrary units (AU). Means ± standard deviation (SD) are indicated.

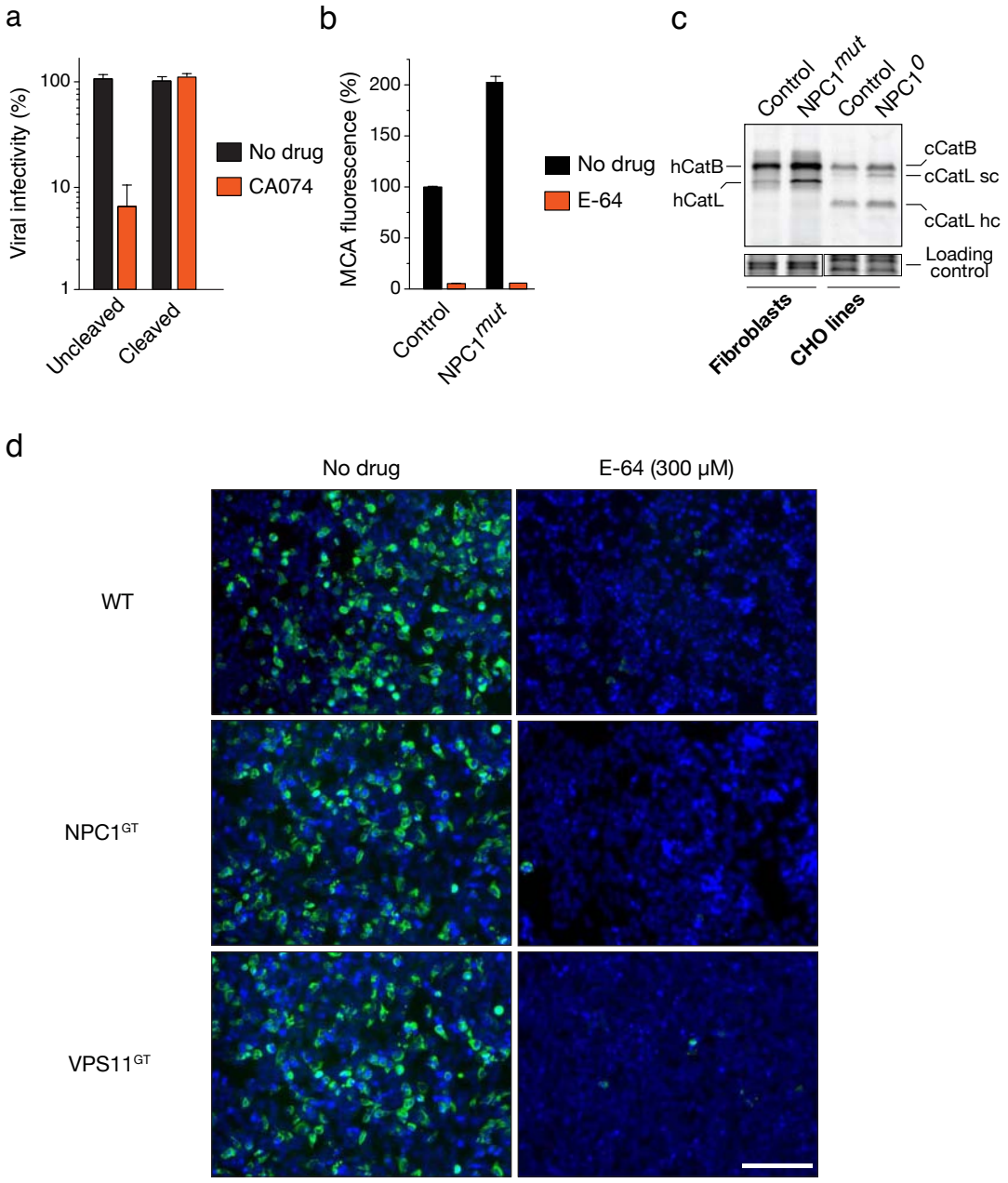

Supplemental Figure 14. The activities of endosomal cysteine cathepsins B and L are not inhibited in NPC1-defective cells. **a**, In vitro cleaved rVSV-GP-EboV bypasses the intracellular requirement for cathepsin B (CatB). Infectivity of mock- or thermolysin-cleaved rVSV-GP-EboV in Vero cells treated with the CatB inhibitor CA074. **b**, Fibroblasts from an apparently normal individual (control) and a Niemann-Pick patient carrying homozygous mutations in NPC1 were lysed at acid pH, and the capacity of these acidic extracts to cleave a fluorogenic peptide substrate for CatB and CatL was measured (see Supplementary Methods for details). Pretreatment of cell extracts with the pan-cysteine protease inhibitor E-64 abolished substrate cleavage, confirming that only cysteine cathepsin activities were being measured. **c**, Intact control and NPC1-deficient fibroblasts and CHO cells were incubated with a cell-permeable fluorophore-tagged suicide substrate that covalently attaches to key catalytic residues in CatB/CatL, a process that requires enzyme activity. Cells were then lysed and fluorophore-labeled CatB and CatL proteins were detected by SDS-polyacrylamide gel electrophoresis and fluorescence imaging. hCatB and hCatL, human enzymes. cCatB and cCatL, CHO enzymes. sc and hc, single chain and heavy chain forms of CatL. **d**, The indicated HAP1 clones were pre-treated with the pan-cysteine cathepsin inhibitor E-64 (300 μM) and then exposed to reovirus T1L virions (MOI 1). Cells were fixed at 24 h post-infection and immunostained for the viral non-structural protein σNS.

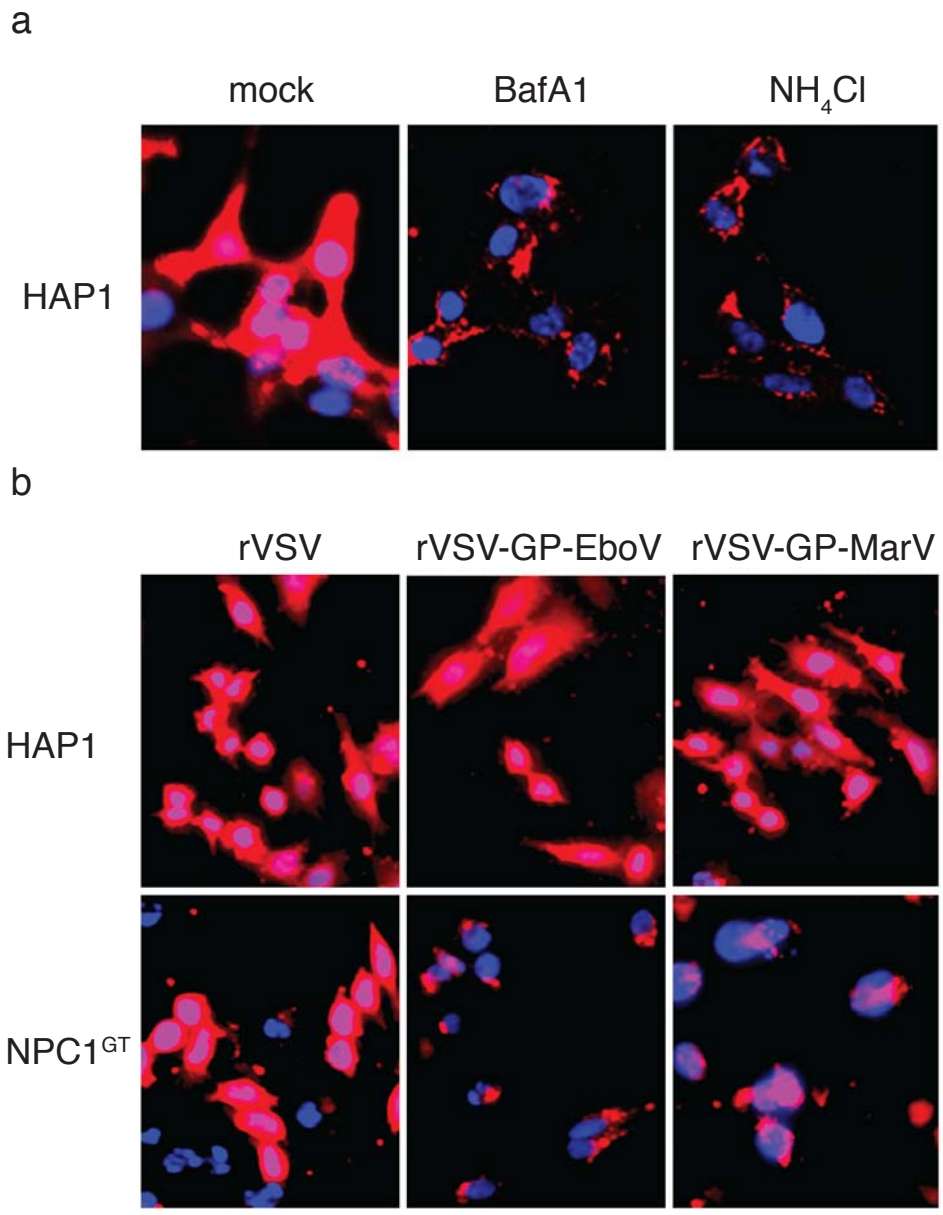

Supplemental Figure 15. Viral membrane fusion mediated by Ebola and Marburg glycoprotein requires NPC1. **a**, Wild type HAP1 cells were treated with puromycin (5 μg/ml) and inoculated with rVSV-GP-EboV in the presence or absence of bafilomycin A1 (bafA1; 100 nM) or ammonium chloride (NH4Cl; 20 μg/ml). Cells were fixed 3 h post inoculation and stained with VSV M antibody 23H12 as described in Methods. Successful fusion leads to the diffuse M staining (red) throughout the cytoplasm. Failure to fuse leads to discrete puncta of M staining as shown by bafA1 and NH4Cl. **b**, Wild type HAP1 cells and NPC1-deficient cells were treated with puromycin and inoculated with rVSV, rVSV-GP-EboV, or VSV-GP-MarV for 3 h and processed for VSV M staining as indicated above.

a

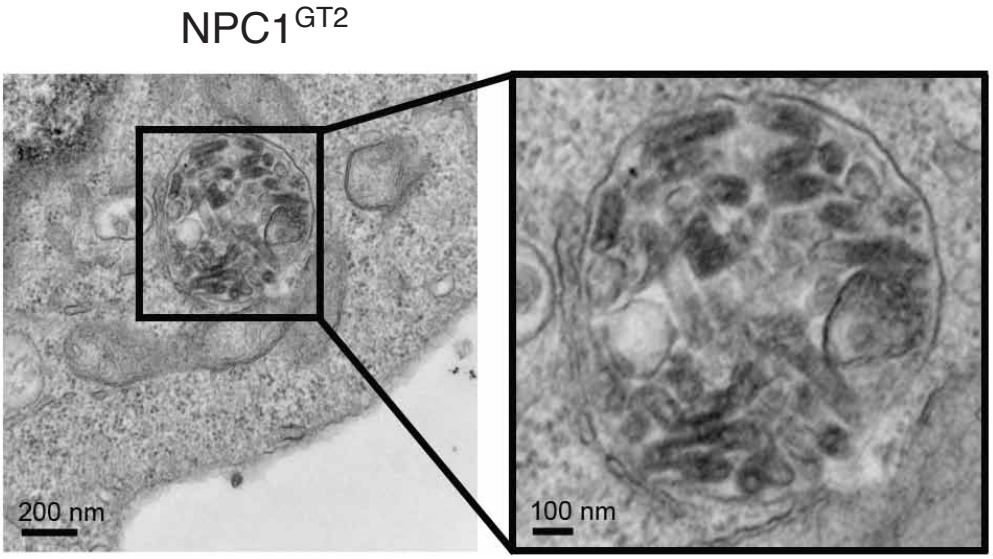

b

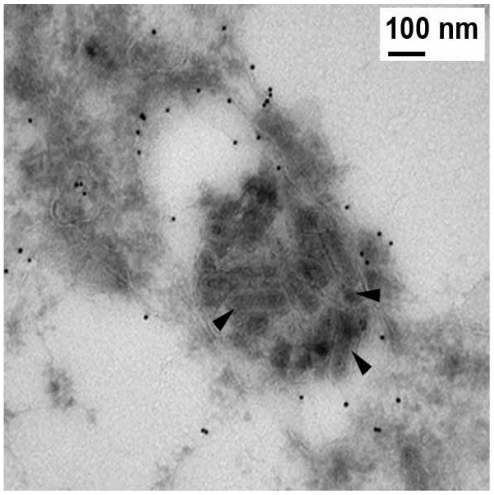

Supplemental Figure 16. Accumulation of rVSV-GP-EboV viral particles in vesicular compartments in NPC1-deficient cells. **a**, Electron micrograph of a second NPC1-deficient HAP1 clone infected with rVSV-GP-EboV. A large agglomeration of bullet-shaped VSV particles is visible within a vesicular (endosomal) compartment. The image was taken 3 h post-infection. **b**, NPC1-deficient HAP1 cells were inoculated with rVSV-GP-EboV and processed from cryo-immunogold electron microscopy as described in Methods. A representative image is depicted. Multiple viral particles (as indicated by the black arrows) can be detected in individual LAMP1-containing structures.

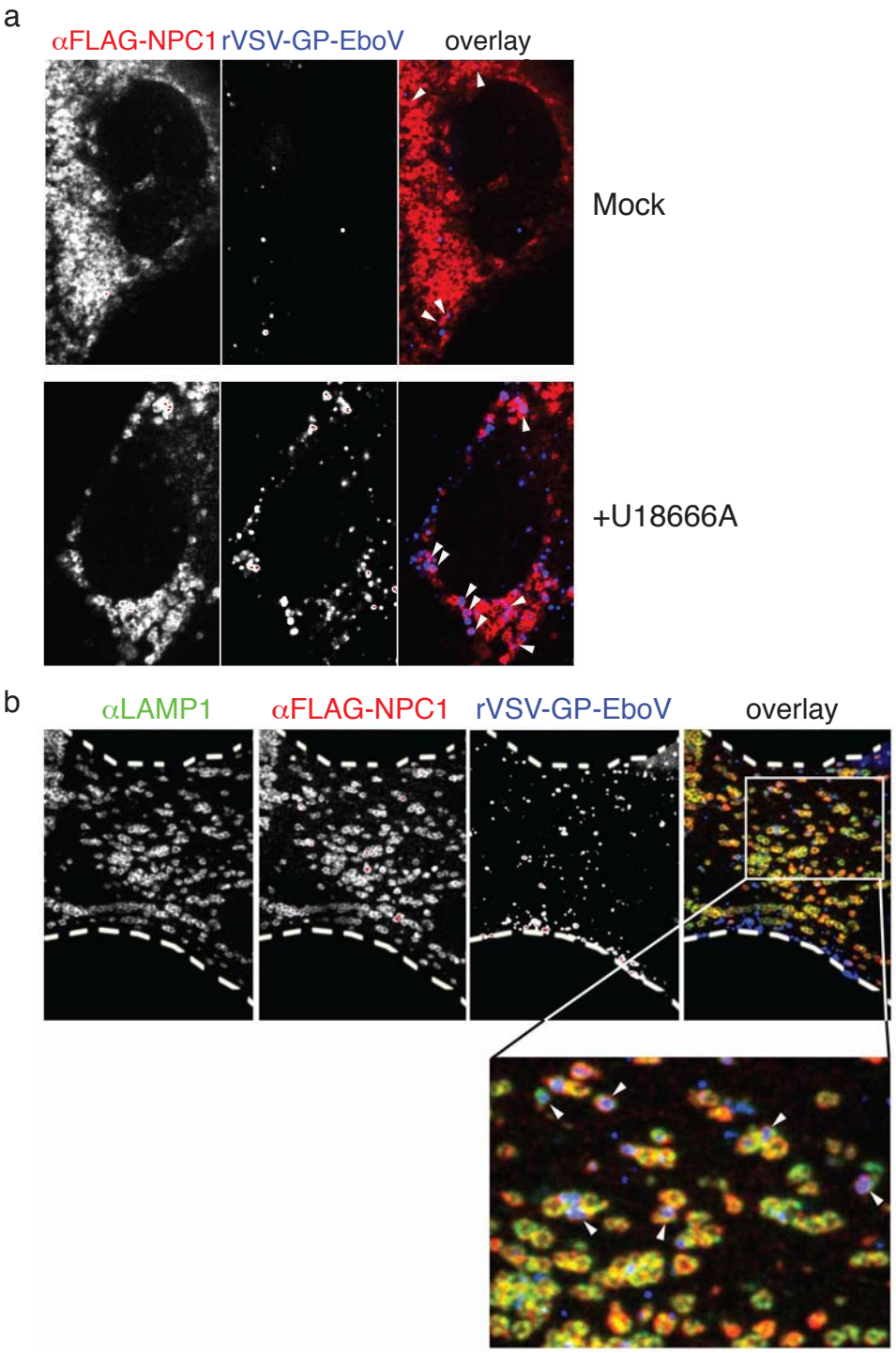

Supplemental Figure 17. Viral particles accumulate in NPC1- and LAMP1-positive endosomes in U18666A-treated cells. **a**, NPC1-mutant fibroblasts were transduced with a retrovirus directing the expression of NPC1 containing a Flag tag. Cells were exposed to Alexa 647-labeled rVSV-GP-EboV (blue) for 3 h in absence (mock) or the presence of 10 μg/ml U18666A. Subsequently, the cells were fixed with 4% PFA and immunostained with antibodies directed against the Flag tag (red). The degree of colocalization of NPC1-Flag with labeled rVSV-GP-EboV was determined on a pixel-to-pixel basis of individual regions of interest using the JACoP plugin in ImageJ software (mock; Pearson's coefficient: 0.094 ± 0.015, U18666A; Pearson's coefficient: 0.42 ± 0.14). **b**, In parallel, cells (exposed to Alexa 647-labeled rVSV-GP-EboV in the presence of 10 μg/ml U18666A) were stained with antibodies directed against the Flag tag (red) and LAMP1 (green) to visualize NPC1- and LAMP1-positive endosomal compartments (Pearson's coefficient: 0.894 ± 0.054).

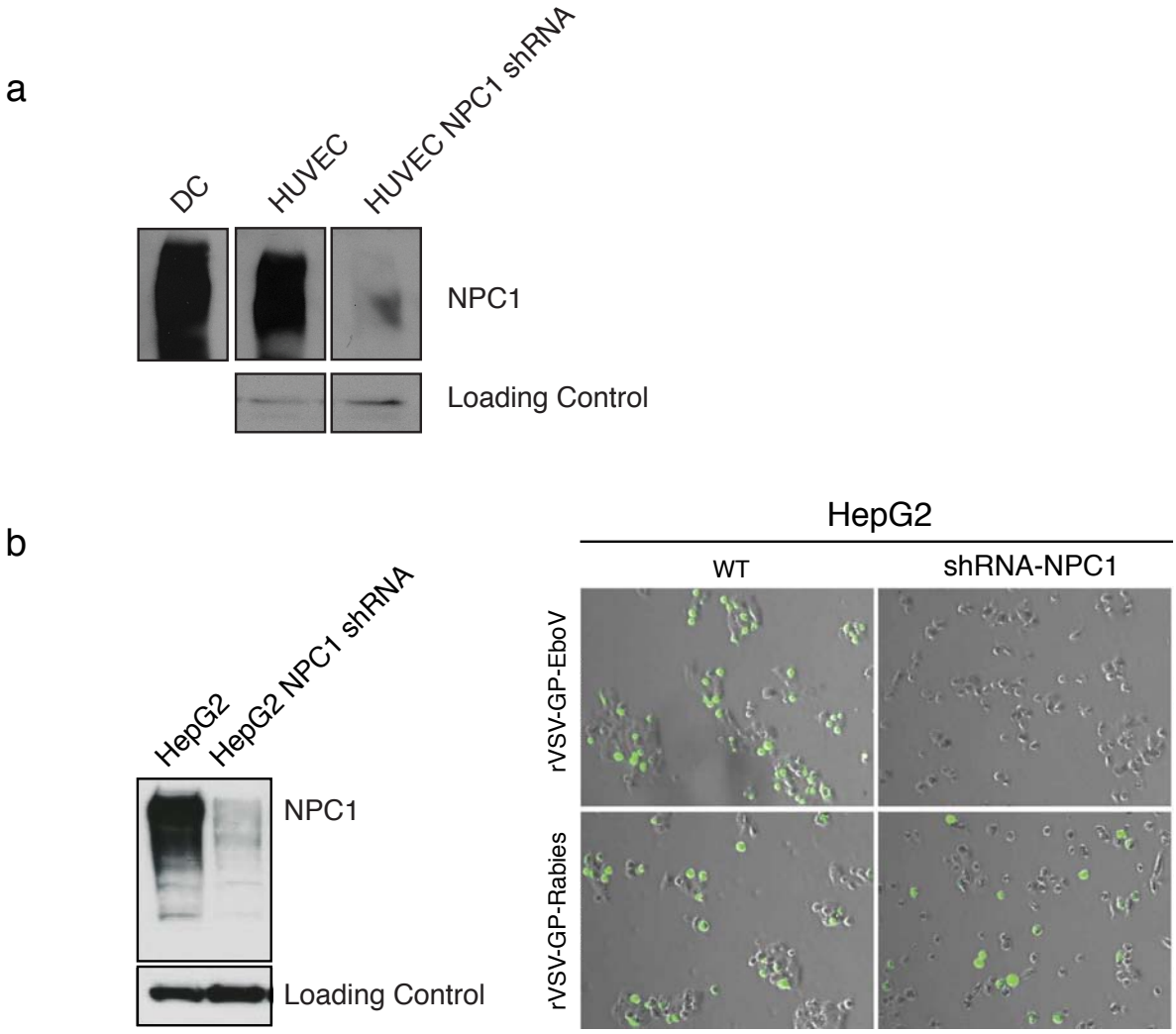

Supplemental Figure 18. NPC1 is expressed in human primary dendritic cells, endothelial cells, and a human hepatocyte cell line, and is necessary for viral infection of these cells mediated by the Ebola virus glycoprotein. **a**, Immunoblot analysis of primary human dendritic cells (DC) and endothelial cells (HUVEC) for expression of NPC1. HUVEC transduced with a lentivirus encoding an NPC1 shRNA express lower amounts of NPC1 relative to cells transduced with a non-targeting shRNA vector. Parallel samples were blotted for β–actin as a loading control. **b**, shRNA-mediated knockdown of NPC1 in HEP-G2 cells (left) impairs infection mediated by the Ebola virus glycoprotein but not by the rabies virus glycoprotein (right).

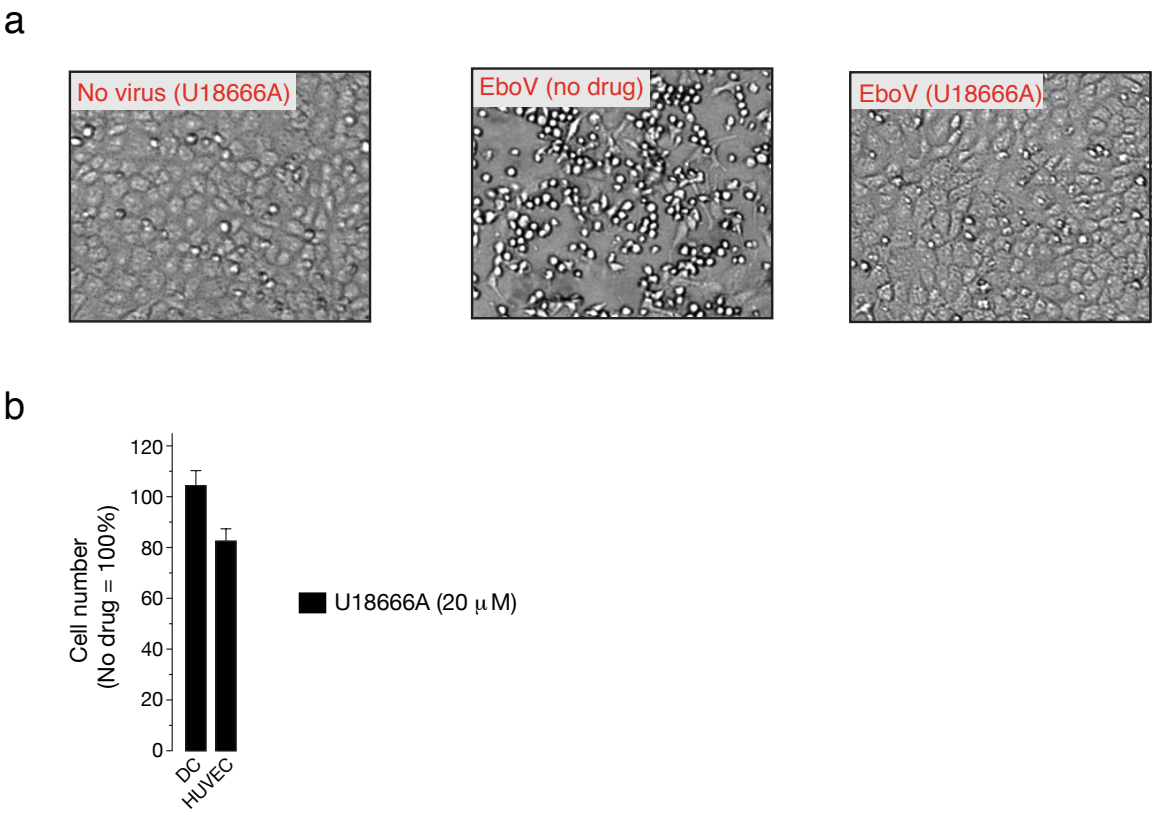

Supplemental Figure 19. U18666A is not cytotoxic to primary and cultured cell types under the treatment conditions employed in this study. **a**, Cells from the experiment in Figure 4c were photographed on day 4. U18666A was not markedly cytotoxic to cells even upon prolonged treatment. Moreover, virus-induced cytopathic effects were evident in untreated cells but not drug-treated cells infected with EboV. **b**, U18666A does not cause marked cytotoxicity in primary DC and HUVEC after 48 h of treatment.